Investigation of Bismuth Doping and Electrolytes on the Photoactivity and Photostability of ZnO Nanorods

Abdulhakeem Oluwadare Adefioye

B.Sc (Chemical Engineering, University of Lagos, Nigeria)

Supervised by:

Dr. Chang Wei Sea (Main supervisor)
Prof. Chai Siang Piao
Dr. Lim Boon Han (UTAR)

A Thesis submitted for

the degree of Master of Engineering Science at Monash University in 2020

Department of Mechanical Engineering, Faculty of Engineering

COPYRIGHT NOTICE

DECLARATION

This thesis contains no material which has been accepted for the award of any other degree or diploma at any university or equivalent institution and that, to the best of my knowledge and belief, this thesis contains no material previously published or written by another person, except where due reference is made in the text of the thesis.

Abdulhakeem Oluwadare Adefioye

October 2020

ACKNOWLEDGEMENTS

I want to use this medium to show immense gratitude to the people that made my intellectual journey in Monash University, Malaysia, a reality, a success, and a fulfilling experience.

First and foremost, I would like to show sincere appreciation to my supervisor, Dr. Chang Wei Sea for giving me the opportunity to explore an intellectual adventure that have changed my life in the most astonishing way. I have learnt the art and science of curiosity, the ability to unleash skepticism at every information that I come across ─ all these thanks to the availability of unprecedented access to the totality of human knowledge on a flash which for the most part I have lacked as an indigent citizen in Nigeria. More provincially, she has also served passionately and adroitly as a co-sailor for steering the wheel of the research project safely especially during the turbulent times. This has been unarguably a watershed moment in my intellectual history and there is no doubt that she would forever be remembered for ushering me into a world reeling with a better understanding of science, reality, and the world.

By the same token, there are also some important personalities that have given me some sort of crucial support during my research project. Mr. Carvyn Blaise for teaching me how to characterize my synthesized samples and even providing the most needed help when I was to meet some important deadlines; he is indeed a gentle, selfless, and marvelous soul. Mr. Kah Tan Hui for providing useful feedbacks in the analysis of results. Mr. Lim Fan Cheng for giving instructions for my first important steps when I was learning the ropes of nanomaterials synthesis and characterization. He gave useful advice and knowledge that helped create the foundation upon which the research was built upon; he made an indelible mark on this project. In addition, I would also be extending my special thanks to Mr. Azaruddin and Mr. Afiq from Nano-Analytical Platform (NAP) for their help with using characterization equipment. Ultimately, I want to express profound gratitude to Monash University, Malaysia for endowing me with a scholarship that helped to support me financially during my study.

Also, I want to show my gargantuan regard to my parents for sacrificing so much for me in sweats and toils just to allow me to have what they or any member of the entire family never had─ a quality education. They have uncontending rights to share with me the victories of my educational adventure. I also want to thank Mr. Alliyu Mubarak for being a part of my educational success stories. We met in my first year as an undergraduate student at University of Lagos, Nigeria. Since then, he has graduated from being a friend to a brother. He has been and still a pillar of support morally, financially, emotionally, and intellectually. He has refined

my thoughts and my attitudes toward learning, supported me financially through my hurdles during my bachelors' studies consequently making it easy for me to divert my focus from hunger towards learning. He continues to make so much sway in my aspiration to being a fountain of impact for my immediate household and a responsible global citizen. On a final note, I want to express my utmost regard to Miss. Shola Adeniji for providing the needed emotional support to having a work-life balance. I hope we can both build a future rich in love and harmony with our families, communities, and mother nature.

Thank you.

Abdulhakeem Oluwadare Adefioye

Table of contents

Table of Figures

Abstract

Zinc oxide (ZnO) nanorod (NR) array is a direct wide bandgap material with the ability to absorb UV light which accounts for 5% of the solar spectrum. This relatively low light absorption has limited their applications for solar water-splitting. Deliberate doping and morphological tuning have been widely used to broaden the optical absorption of ZnO NRs. Two approaches employed in this study are the effect of bismuth concentration and growth time on the optical and photocatalytic ability of ZnO NR. It was affirmed that 2%wt doping level of bismuth was critical to improving light absorption and photocurrent response of ZnO NR array by 37%. Nevertheless, photocurrent gain resulting from bismuth addition was lost to chemical dissolution of ZnO NR over a 1 h period in 0.5M Na_2SO_4 solution as depicted by EIS analysis. Subsequently, the use of carbonated buffer (CB) was proposed as a viable candidate for mitigating chemical dissolution and photocurrent decline of ZnO NR. PEC characterization was performed to compare 0.025M CB and sulphate solution based on how they affect photoresponse and photostability of pure and doped ZnO NR. Analysis of results revealed that, sulphate solution has deleterious effect on photocurrent stability while carbonated buffer has twin advantages of suppressing chemical dissolution and preserving photocurrent gain occasioned by 2%wt bismuth addition by 17% over 1 h. This hereby suggests that carbonated buffer is superior to sulphate solution for photoelectrochemical water-splitting application.

Chapter 1 Introduction

1.1 Background

ZnO is an attractive candidate that can be used to generate hydrogen gas by utilizing radiation from sun. It is a semiconductor that responds primarily to UV component of sunlight due to its inherent large bandgap (~3.3 eV). The electron affinity and energy bands of ZnO are like TiO_2. Moreover, the recombination of the photoinduced charge carriers occurred quickly on a time scale of 10^{-9} to 10^{-12} s. To utilize visible light and enhance the photoactivity of nanomaterials, the development of highly efficient and visible light responsive photocatalyst is crucial[1].

One of the intriguing properties of nanostructured materials is the existence of chemical reaction at the surface of the materials. This has drawn attention of researchers to nanomaterials and particularly hierarchical structures with geometric complexity or multiple constituents. 1D nanomaterials[2,3] offer an amazingly huge and ion-available surface site. The nanotubular configuration prompts an augmentation in reactivity and specific reaction rates[4,5]. From the perspective of photoconductivity, one of the points of interest arising from their structure is their free carrier movement, which comparably is much slower than in nanoparticle systems. 3D nanostructures have a relatively large specific surface area, higher photocurrent response and smaller density. Such exceptionally permeable morphology provides the vital robustness, which have the potential to result in maximal utilization of the huge portion of irradiated light and high level of ion diffusion in electrolyte[6–8].

Photoelectrochemical (PEC) systems are expected to be made of a photoelectrode with large interfacial contact area with the electrolyte. Polycrystalline photoelectrodes that are not single crystals usually contain structural defects. It is commonly believed that defects serve as recombination sites where annihilation of photoinduced electron-hole pairs occur. This disadvantageous property provides the need to use single-crystal nanostructures for PEC systems. Different types of ZnO nanostructures such as nanofilms, nanorods, nanobelts and nanoflowers have been reported in literatures. ZnO nanostructures have a high surface-to-volume ratio which play a significant role in their chemical reactivity to sunlight resulting in dramatic change in their optical, electrical and mechanical properties[9,10].

With regards to photoconductivity, ZnO NR (1D nanomaterial) has attracted interests of academic researchers because it offers impressive capabilities such as large surface area for enhanced reactivity, efficient charge transport due to its defined characteristic length that guides charge carrier mobility. However, ZnO NR is not without its deficiency; It reacts

primarily to ultraviolet spectrum of light and several strategies have currently been explored to continue to further stretch its photocatalytic activity.

The photoactivity of ZnO has been enhanced by a battery of strategies such as modulation of ZnO by dye sensitization[11], transition metals doping [12], non-metal doping[13], and use of sandwiched semiconductors, etc. Interestingly, some of these approaches have been successful. Improved photocatalytic reactions and redshift of photoresponse have been witnessed for various coupled ZnO systems [14–16]. In the deployment of performance-driven approaches in the synthesis of ZnO, the literatures are replete with a suite of physical and chemical techniques.

In this study, the use of doping was adopted as a strategy for improving the PEC performance of ZnO NR. There are comprehensive and well-documented literatures on the augmentation of photoresponse of ZnO using all sorts of dopants such as transition metals(Ag, Mn, Cu, Fe), rare-earth metals(Ce, La), non-metals(N, C, S). In the light of this, this study particularly focused on the impact of bismuth— a group V element— on the PEC performance of ZnO NR. It is noteworthy to mention that previous research works have delved greatly into doping of ZnO film with other group V elements such as N, P, As and Sb. These dopants can improve conductivity of ZnO films while also imparting stable n-type and p-type conductivity thereby making ZnO suitable in the optoelectronic industry. Despite the impressive properties imparted by group V elements, their counterpart bismuth appears to be fraught with some issues especially as it concerns improving the properties of ZnO films. The most common challenges as documented in literatures are phase separation leading to high resistivity of ZnO and its inability to induce p-type conductivity in ZnO. These challenges have been addressed by using very low concentration of bismuth to solve the problem of phase separation, and a later approach building on this understanding to synthesise a p-type ZnO film using pulse laser deposition[17].

Apart from the enhancement of the PEC performance using doping, it is also essential to ensure the preservation of photocurrent generated by nanomaterials. In fact, the decline in photocurrent after prolonged light exposure—popularly regarded as photocorrosion has been posited as one of the biggest hurdles faced in the fabrication of efficient water-splitters[18]. The use of stable electrolytes has been revealed to be effective in suppressing photocorrosion whilst preserving photocurrent. Therefore, to the best of the author's knowledge, for the very

first time, the study hereby attempted to explore the influence of bismuth dopant and stable electrolyte on hydrothermally based ZnO NR.

1.2 Problem statement

ZnO NR array has a theoretical bandgap of 3.3 eV implying that only photons with wavelength ranging from 300 nm to 400 nm can be absorbed by ZnO NRs. This leaves photons with wavelength range above 400nm accounting for about 95% of the solar spectrum to be unutilized by ZnO NRs. To overcome this challenge, doping of ZnO NRs with bismuth using hydrothermal method was employed with the goal of expanding the sensitivity of the material to visible spectrum of solar radiation. Also, the use of electrolyte was used in examining the effect of chemical dissolution on the photoresponse of ZnO NRs.

1.3 Research objectives

This research is focused on twin objectives, broadening the wavelength range absorbed by ZnO NRs and suppressing the effect of chemical dissolution with the view to sustain the PEC performance of ZnO NRs over an extended period. To achieve this, ZnO NRs and a range of bismuth doped ZnO NRs would be fabricated on a FTO substrate. Structural, optical, and electrochemical characterization were performed to study crystalline, morphological, and photocatalytic properties of the as-synthesized materials. Lastly, conventional characterization methods were also employed in understanding how electrolyte affects the photoactivity and photostability of ZnO NRs. Several factors will be systematically studied as listed in the followings:

1) Investigating the influence of bismuth concentration on PEC performance of ZnO NRs
2) Studying the effect of growth time on PEC performance of ZnO NRs
3) Investigating the effect of electrolyte on PEC performance and photostability of ZnO NRs

Chapter 2 Literature review

2.1 Introduction

Nanomaterials have pulled in monstrous enthusiasm because of their amazing presentation in photonics, optics, and electronics. Nanomaterials have three major types based on dimensionality: 0D, 1D, and 2D. 1D nanostructures are helpful materials for testing the relationship of electrical, transport, thermal and mechanical properties on size decrease and dimensionality [19]. Among the 1D nanostructures, zinc oxide (ZnO) NWs—used interchangeably with ZnO NRs—is one of the essential nanomaterials in the nanotechnology space in today's research [20]. It has fascinating chemical and physical properties. For example, high chemical stability, high photostability, high electrochemical coupling coefficient and relatively wide gamut of absorbed radiation. All of these properties offer the materials multi-dimensional functionalities[21]. In the material world, ZnO is typified as a group II-VI semiconductor, which is on a borderline between ionic and covalent semiconductors.

There exists an enormous fascination in ZnO materials lately, based on the massive increase in the number of publications referring to this amazing material and its excellent property. The attraction for ZnO is fuelled by its promising usefulness in optoelectronics industry owing to its direct large bandgap (3.3 eV) at 300 K. ZnO has a large exciton binding energy (60 meV) at room temperature[22]. ZnO is also biocompatible, biodegradable and safe for environmental and medical uses[23]. Due to their wonderful performance in photonics, electronics, and optics, ZnO NRs are attractive candidates for many applications such as UV lasers [24], light-emitting diodes[25], solar cells [26], nano-generators [27], gas sensors[28], UV photodetectors[29] and photoelectrochemical water splitting[30].

Photoelectrochemical (PEC) water splitting employing nanostructured materials is one of the amazing techniques used to address the storage challenge that comes with the harvesting of solar energy. This is achieved using a photocatalyst (also called artificial leaf) in splitting water molecules to produce hydrogen in an easier, cheaper, and sustainable way. By modifying a photocatalyst to get a suitable bandgap, the overall STH energy conversion efficiency can be improved. Nanomaterials' bandgap can be tuned by controlling its size, morphology, and intentional doping process.

It is common knowledge that solar energy is free, inexhaustible, clean, and sustainable form of energy asset on our planet. Every year, the measure of sunlight-based energy arriving at our planet is around 100000 Terawatts (TW), of which around 36000 TW arrives at the land. This hence suggests pretty much 1% of natural land should be secured with simply 10% efficient

PEC cells to deliver 36 TW every year, and is sufficient to fulfill anticipated worldwide yearly energy utilization in the year 2050[31]. Hence, the essential need to harness immense energy from the sun. In recent times, artificial photosynthesis is being used to harvest solar energy to deliver energy-dense chemical fuels such as hydrogen or hydrocarbons through alternative processes such as water splitting or CO_2 utilisation. Among the different chemical fuels, hydrogen's energy density per mass compared to gasoline is higher by a factor of 3 or 4 and can be utilised in automobile combustion engines, fuel cells and finally in the processing of common chemicals. Despite the progress made thus far by this technology, there is still a challenge in the construction of efficient and stable solar-to-hydrogen (STH) energy transformation device. Even though water splitting devices have been accounted to work with a 30% STH efficiency through combination of an electrolyser and photovoltaic cell [32]. Currently, research is now geared towards the improvement of cost effective and stable water-splitting PEC cells.

The driving forces behind STH conversion are one, a small over-potential critical to driving the water splitting process. Although several PV cells are made in series arrangement to reach the base potential (3.0 V required by the electrolyser in an indirect route). Secondly, the water splitting reaction requires a much simpler, cost-reducing and space-reducing construction with fewer physical components like wires, reactor, and electrodes, etc.

Policy makers and academic researchers are emphasizing efforts in the direction of sustainable energy resources to address the anticipated dearth of traditional and non-renewable energies and its concomitant environmental devastation. Hydrogen is one of those fuels with zero emission of pollutants when combusted in oxygen-laden environment. It is a promising renewable fuel, used in automobiles, aircraft, spacecraft propulsion and electric devices.

There are various ways to get hydrogen through water-splitting methods. In 2017, Bu *et al.* defined water splitting as a process of cleaving hydrogen bonds in water to form hydrogen and oxygen. Different methods for water splitting have been issued like photoelectrochemical (PEC) [33] photocatalytic[34], radiolysis[35], photo-biological [36] and thermal decomposition[37]. Radiolysis ejects by-product containing nuclear waste[35]. In principle, photo-biological water-splitting is with the help of an algae bioreactor, it shifts from oxygen production (normal photosynthesis) to producing low-H_2 evolution rates[36].

2.2 Zinc Oxide

2.2.1 Crystal structure

ZnO is a group II-VI binary semiconductor compound that can crystallize into three morphological forms which are hexagonal wurtzite (WZ), cubic rocksalt(RS) and zinc-blende(ZB) structure. WZ is the most thermodynamically stable phase at ambient conditions while RS and ZB are metastable at ambient conditions. In the crystallography of WZ and ZB structure, each Zn (or O) is attached to four neighbouring atoms. The angles of adjoining tetrahedral units are 60^0 and 0^0 for ZB and WZ, respectively. Contrastingly, in RS structure, each Zn (or O) is attached to six neighbouring atoms with a zero-degree angle for adjacent tetrahedral units. This tetrahedral coordination is peculiar to sp^3 covalent bonding albeit these materials are on the borderline between ionicity and covalency[38,39].

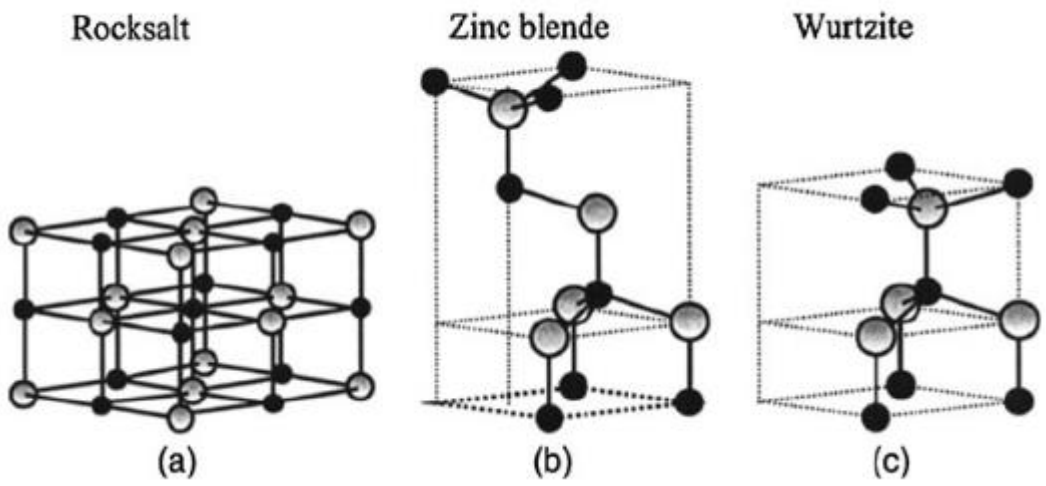

Figure 2.1: ZnO crystal structure: Shaded gray and black balls represent Zn and O atoms. (a) cubic rocksalt (b) cubic zinc blende (c) hexagonal wurtzite[38]

2.2.2 Phase transformation of ZnO

A number of studies have been launched into the phase transformation of ZnO that is WZ-RS transition and WZ-ZB transition. This is credited to the unusually interesting transport and optical properties of metastable RS and the expectation of metastable ZB to be suitable for use in a myriad of device applications based on characteristics such as lower carrier scattering, higher doping efficiencies. These outstanding features have been attributed to higher symmetry in the zincblende crystallographic structure[40,41]. In 1962, Bates *et al.* for the first time reported the influence of pressure on phase transition from WZ to RS structure[42]. The high-

pressure performance of nanocrystalline ZnO with a mean grain size of 12 nm was explored by in-situ high-pressure synchrotron radiation X-ray powder diffraction, electrical resistance, and optical measurements. It was revealed that the conversion pressure of the WZ-to-RS phase change rises from 9.9 GPa for bulk ZnO to 15.1 GPa[43]. Haozhe *et al.* using a high resolution angular dispersive x-ray diffraction in a helium pressure medium showed that WZ-to-RS transition occurs between 8.8 to 15.5 GPa[44]. Jamieson proved experimentally WZ-RS transition to be reversible using in-situ X-ray diffraction at room temperature [45]. Decremps *et al.* demonstrated the capture of RS-ZnO at ambient condition after annealing at high pressure of 15 GPa and 550 K. Analysis of the recovered sample using X-ray absorption spectroscopy(XAS) and X-ray diffraction(XRD) detailed the nature of the sample through probing its long-range order and crystallographic structure[46].

Pressurised doping process has also proven effective in the ZnO phase transformation. Wang *et al.* performed WZ-to-cubic phase transformation of ZnO by doping with manganese(Mn)—An attempt to study the effect of transition metals on WS-cubic transition. The outset transition pressure for the process declines from about 9.5 GPa to 6 GPa for pure ZnO and sintered 2at.% Mn-doped ZnO, respectively. Investigation was carried out using synchrotron radiation in in-situ high pressure X-ray powder diffraction. It was observed that Mn ions occupies the Zn site in the WZ structure while also asserting that Mn doping shrinks the phase transformation barrier [47]. On the other hand, experimental efforts toward the formation of stable ZB-ZnO phase have been achieved through heteroepitaxial growth on different kinds of substrate using methods like molecular beam epitaxy, thermal oxidation, and sol-gel process. Ashrafi *et al.* deposited the ZB-ZnO films on GaAs(001) substrates by metalorganic molecular beam epitaxy using ZnS buffer layers. The ZnS buffer layer helped to ensure a high crystal quality of ZnO layers whilst making sure the stability of ZB-ZnO on GaAs substrate. This was achieved through the prevention of the creation of the amorphous oxide films on GaAs surfaces and decrease of lattice mismatch in the ZnO/GaAs heterostructure. Stable ZB-ZnO films were successfully deposited on ZnS/GaAs substrate at temperature of 400 °C to 600 °C[48]. Lee *et al.* grew ZB-ZnO film by thermally oxidizing ZB-ZnS film deposited epitaxially on a sapphire (0001) substrate at 900 °C under O_2 stream for 2 h. Pulsed laser deposition (PLD) of the ZnS film was performed at 800 °C under working pressure of 7×10^{-7} Torr. At the end of the oxidation process, XRD can be used to characterise crystallographic structure of the as-synthesized sample. The result showed the disappearance of ZnS diffraction peaks but showed predominant peaks of (002) and (004) for WZ-ZnO and ZB-ZnO layers respectively[49]. Kim

et al. stated that the growth of a ZB-ZnO on Pt(111)/Ti/SiO_2/Si substrate using sol-gel synthesis at a temperature above 700 °C. The study also showed that ZB-ZnO could be supressed leading to WZ-ZnO crystal by using Pt(111)/TiO_2/SiO_2/Si substrate instead of Pt(111)/Ti/SiO_2/Si substrate. Likewise, it was proven that WZ-ZnO predominates at temperatures below 700 °C [50]. Chichvarina *et al.* investigated the fabrication of ZB–ZnO thin layers on substrates with the following arrangement Pt/Ti/SiO_2/Si. WZ-ZB phase transition was observed for PLD of the ZnO film after 900 °C heat treatment at a working pressure of 8×10^{-4} Torr. 20nm thickness of deposited ZnO film was shown to be critical in the formation of ZB phase. Beyond 20nm, the mixture WZ, ZB and Zinc titanate (Zi_2TiO_4) phase were observed. The study further revealed that below 20nm, out-diffusion of Ti promotes ZB phase while Pt under layer is responsible for stabilization of ZB phase[51]. Ultimately, in all synthesis routes required in the synthesis of ZB phase, it is difficult to achieve a purely single-phase ZB phase due to the propensity to form WZ subcategories within the ZB crystal even though it is an essential issue of concern due to several technological benefits over WZ.

2.2.3 Properties of ZnO

The vast gamut of advantageous characteristics exhibited by ZnO have been seen for quite a while now. What has arrested most of the attention of late is the fact that ZnO is a semiconductor with a direct bandgap of ~3.3 eV[1], which on a basic level empowers optoelectronic uses in the UV and blue regions of the visible spectrum. The potential of such functions has been powered by remarkable advancement in bulk-crystal[52,53] together with thin-film proliferation in the course of recent years [54,55]. Coming up next is an inexhaustive rundown of the features of ZnO that makes it unique as a semiconductor or oxides.

1) High thermal conductivity

This property makes ZnO valuable as an added substance (For example, ZnO is used as an additive in rubber to augment thermal conductivity of tires). It additionally expands the allure of ZnO as a substrate for heteroepitaxy or homoepitaxy (For example, for development of GaN, which has fundamentally comparable lattice constant) [56,57]. Elevated conductivity turns into enhanced efficiency of heat depletion in the course of operating device [58]

2) Large band gap

ZnO bandgap sometimes varies based on nanostructures, processing techniques, operating conditions, etc. Hence, the bandgap at small temperatures and room temperatures are 3.44 eV and 3.37 eV, respectively[59]. For the sake of comparison, bandgap values for wurtzite is 3.50

eV and while 3.44 eV is for GaN[60]. The afore-stated values above facilitate applications in optoelectronics in the UV/ blue spectrum, including photodetectors, light-emitting diodes and laser diodes [38,61]. ZnO platelets[62], ZnO thin films [63], ZnO nanowires [64] and ZnO nanocrystal clusters[65] have been reported to be used for optically pumped lasing. Publications on p–n homojunctions have recently emerged in scientific literatures [66–68], however, reproducibility and stability issues have not yet been solved.

3) Availability of single big crystals

One of the most appealing highlights of ZnO as a semiconductor is that large facet single crystals are obtainable, and epi-prepared substrates are currently on the market. Bulk crystals can be developed with an assortment of synthetic methods, comprising hydrothermal growth [53,69], vapor-phase transport [70] and pressurized melt growth [71,72]. Development of thin films can be achieved using chemical vapor deposition(MOCVD) [73], laser ablation [74] and molecular-beam epitaxy[75]. High-quality thin films with lowered density of prolonged defects can be produced via the epitaxial growth of ZnO on substrates. This is particularly noteworthy when contrasted with GaN, for which there is no existence of native substrates. Considering the fact that devices built with GaN have accomplished incredible efficiencies despite the comparatively large concentration of extensive defects, there is a potential to build superior ZnO-based device with efficiencies greater than that of GaN.

4) Strong Luminescence

Because of the intense luminescence in the green–white portion of the visible spectrum, ZnO serves as an appropriate material for light emitting diodes(LED) applications. The spectral emissions peak at 495nm and 0.4 eV large half-width [76]. The n-type conductivity of ZnO makes it appropriate for applications in vacuum fluorescent displays and field emission displays. There has been a lot of controversies in the field, and very little understanding has forged so far on the source luminescence. In addition, luminescence mechanisms have been developed and the phenomenon has been attributed to zinc interstitials and oxygen vacancies, this has been supported with tenuous evidences[76]. These defects do not emit light in green region. However, it has been recommended that zinc vacancies are more likely to be the source of the green luminescence. Zn vacancies are acceptors and can readily form p-type ZnO.

5) Wide exciton binding energy

This huge exciton binding energy suggests that there would be a preservation in the efficiency of excitonic emission at room temperature and even greater temperatures[62,63]. The binding energy of free excitons in ZnO is 60 meV. It has been garnered that oscillator strengths of electron–hole transitions in direct bandgap semiconductors are generally much lower than that of excitons[77]. This fascinatingly huge exciton binding energy renders ZnO a useful material for optical devices that are centred on excitonic effects.

6) Strong non-linear resistance of polycrystalline ZnO

ZnO varistors that are available on the market are made of polycrystalline films with high non-ohmic I-V characteristics. The non-linear resistance feature of ZnO has frequently been ascribed to grain boundaries. However, the microscopic mechanisms are not fully understood. In addition, the influence of microstructures and additives on the degradation of material remains a subject of discussion[78].

7) Amenability to wet chemical etching

The fabrication of ZnO-based devices significantly gains from the pliability to low-temperature wet chemical etching. There has been a myriad of reports on etching ZnO thin films using alkaline, acidic, and mixed solutions. The use of low-temperature chemical etching procedure makes ZnO-based devices adaptable to design and integration of optical and electronic gadgets.

8) Strong sensitivity of surface conductivity to adsorbed species

The conductivity is exceptionally sensitive when surface of ZnO thin films is introduced to different gases. It has been extensively used in the food and beverage industry for testing the freshness of products. This property has been linked to its sensitivity to the presence of trimethylamine in the odour [79]. The mechanics of sensing remains a knotty issue with little conception. Late investigations uncover a startling observation showing that an annealed single crystal in vacuum has a surface electron accumulation layer, which vanishes in ambient air [80–82]. This bizarre layer may assume a function in sensing activity. Also, The existence of this conductive surface has been proposed to be linked to some perplexing type-transformation effects witnessed in an attempt to generate p-type ZnO [80–82].

9) Large piezoelectric constant

ZnO is piezoelectric in nature. The deformation of ZnO can lead to the generation of potential bias and vice versa. ZnO materials are typically utilized in as transducers, sensors, and

actuators. ZnO has a combination of features such as high electromechanical coupling and low-symmetry wurtzite crystal structure gives rise to large pyroelectric and piezoelectric effects. Piezoelectric ZnO films with uniform thickness and orientation have been grown on a variety of substrates using different deposition techniques, including sol–gel process[83], spray pyrolysis[84], chemical vapor deposition[85], molecular-beam epitaxy[86].

2.2.4 Synthesis of ZnO using hydrothermal method

In this work, ZnO NR array is explored due to its many advantages when compared to ZnO thin films and nanoparticles. It has relatively larger surface area than thin films and can be coated on a surface. It can vertically align on most substrates leading to improved light absorption due to scattering and high carrier mobility. Lastly, it doesn't require post-treatment, and doesn't run the risk of coalescence or sintering like that of nanoparticles thereby reducing interfacial area for photocatalysis[87].

The fabrication of ZnO NR is basically grouped under two categories, vapor phase method and solution phase method.

Vapor phase method is arguably the most extensively explored technique in the synthesis of 1D nanostructures[88]. A prototypical vapor phase approach takes place a gaseous environment in an airtight container or vessel. As a first step, chemical processes such as evaporation, chemical reduction, and gaseous reaction are used for the formation of gaseous species. Thereafter, the gaseous materials are deposited on a solid substrate by condensation. It is very important to note that vapor phase methods are performed at high temperatures in the range of 500 °C to 1500 °C, leading to the formation of high-quality NW. Conventional vapor phase methods include metal organic vapor phase epitaxy (MOVPE)[89], pulsed laser deposition (PLD) [90], vapor-liquid-solid (VLS) growth[91], metal organic chemical vapor deposition (MOCVD) [92], molecular beam epitaxy (MBE)[93], physical vapor deposition (PVD)[94], chemical vapor deposition (CVD)[95].

However, in this report, ZnO NR is synthesised using a solution approach. The motivation behind the use of this approach is due to its numerous advantages namely low cost, low toxicity in terms of used chemicals, mild temperature, and ease of control and potential scalability. In general, solution synthesis process occurs at significantly small temperatures (< 200 °C) in contrast with vapor phase techniques. As a result, solution phase approaches allow for more flexibility in terms of the choice of substrates comprising organic and inorganic substrates. With regard to the aforementioned advantages, solution-based methods have drawn curiosity

of researchers up till now. Solution-based approach can be used to grow ZnO NRs in an organic or aqueous solution, or a conflation of both solutions[96,97].

2.2.4.1 Hydrothermal method

Hydrothermal synthesis involves the synthesis of materials in a sealed and heated chamber at a temperature and pressure above ambient conditions. In hydrothermal synthesis process, growth of crystal is normally done in a steel pressure container called autoclave.

A typical hydrothermal synthesis for ZnO NRs is performed as delineated below:

1) A certain substrate is selected depending on the intended application of the fabricated device. Substrate could be inorganic or organic-based. After this, substrate is then pre-cleaned in line with established laboratory or industrial practices in order to minimise inefficiency of device caused by impurities.

2) A thin layer of ZnO deposited on the substrate serves as a seed layer. The seed layer provides a site for agglomeration of clusters(nuclei) for the growth of NRs due to the decrease of the thermodynamic barrier[98]. It is also reported that seed layer affects diameter, length, crystallinity, surface roughness and the vertical alignment of ZnO NRs[99].

3) The ZnO seeded substrate is then placed diagonally in a vessel.

4) Chemical reaction is performed in a sealed and heated vessel between Zn cation salt ($Zn(NO_3)_2$, $ZnCl_2$, etc.) and alkaline reagent (such hexamethylenetetramine(HMTA) or NaOH in aqueous solution at a specific temperature and time.

5) After the given time as elapsed, the substrate in the growth solution is then removed and cleaned with deionized water and thereafter dried on a hotplate at ambient condition.

Ladanov *et al.* reported the chemistry of reaction in the sealed vessel as summarized below and this is valid as far as HMTA and zinc nitrate hexahydrate are used as precursors[100]:

1) Decomposition reaction:

$$(CH_2)_6N_4 + 6H_2O \longrightarrow 6HCHO + 4NH_3 \quad (2.1)$$

2) Hydroxyl supply reaction:

$$NH_3 + H_2O \longrightarrow NH_4^+ + OH^- \quad (2.2)$$

3) Supersaturation reaction:

$$2OH^- + Zn^{2+} \longrightarrow Zn(OH)_2 \quad (2.3)$$

4) ZnO nanorod growth reaction:

$$Zn(OH)_2 \longrightarrow ZnO + H_2O \quad (2.4)$$

2.2.4.2 Influence of explanatory variables on ZnO NRs growth

1) Role of Seed Layer: Seed layer is deposited on a substrate using methods such as spin coating, thermal decomposition, physical vapor deposition and sputtering. This is immediately followed by annealing in different environment (ambient or inert). Annealing is performed in order to make the seed crystal adhere strongly to the substrate while also facilitating the vertical alignment of ZnO NRs so as to ensure the efficient transport of charge carriers for collection at the electrode.

2) Role of Alkaline Reagent: Numerous works on hydrothermally based ZnO NRs have been abundantly performed with alkaline reagents like NaOH, Na_2CO_3, KOH hexamethylenetetramine (HMTA), ammonia, and ethylenediamine. Emphasis have been made on the use of HMTA because it is used at very mild temperature below 100 °C and leads to the synthesis of high quality ZnO NRs [101]. By and large, HMTA drives the ZnO NRs growth by buffering pH via slowly releasing hydroxyl ions in order to reduce supersaturation levels[102]. HMTA being a non-polar material gets attached to non-polar planes ((010) and (110)) of the ZnO NRs while promoting growth of Zn^{2+} along the (001) plane along the c-axis[98].

3) Role of temperature: Sugunan *et al.* reported that, by using 1mM precursors(Zinc nitrate hexahydrate and HMTA), there is no significant change in the length of ZnO NRs between temperatures of 65 °C and 95 °C [98]. It was also reported that the length of ZnO NRs varies linearly with temperature between 40 °C and 100 °C, all other factors held constant with 0.025M precursors[103]. There can also be a change in the morphology of the ZnO NRs at relatively higher temperatures. Transformation of ZnO NRs to multipods is achieved from 120 °C to 140 °C [104]. With this observation, it can be inferred that there is significant increase in the mean diameter of the rods at higher temperatures.

4) Role of Growth Substrate: The substrate that is being used for growing ZnO NRs such as FTO and ITO are suited for many applications ranging from photovoltaics to

photoelectrochemical splitting. It is important that they need to meet the following standard criteria; transparency to solar irradiation (more importantly visible portion of the radiation), high conductivity (to ferry electrons easily to the external circuit), stable to electrolytes and high temperatures (as it concerns PEC application), and easy deposition of crystals. Fluorine-doped tin oxide (FTO) and Indium-doped tin oxide (ITO) are generally being used in most reported works as they meet the afore-stated criteria. FTO and ITO are inorganic semiconductors. Other materials however that are used as substrate are polymers, glass, metals and more.

5) Role of precursor concentration: ZnO NRs mean density and diameter are sensitive to operating conditions and therefore increase with increase in reactant concentrations. However, when the precursor concentration is further increased beyond a critical point, the density steadily and infinitesimally increases[105,106]. Rachamim *et al.* also reported that precursor concentration increases non-linearly with diameter up until a critical concentration of 0.07M[103].

6) Role of Growth Time: Yuan *et al.* showed that ZnO NRs average diameter increases with time and peaked at 2.5hours. The authors claimed the growth in size stopped because of the consummation of the precursor chemicals[107]. Baruah and Dutta carried out ZnO NW experiments using different growth durations from 5 to 15 h. It was proved that both length and diameter of the nanowires increased with increasing growth duration time but the aspect ratio was reduced[108]. Although NW growth slowed down after a certain period resulting from depletion of the reacting chemicals. Continual supply of chemicals can be performed to continue the growth rate. However, the increase of average diameter during growth leads to the coalescence of individual rods and finally forms two-dimensional ZnO films.

2.3 Photoelectrochemical Water Splitting

2.3.1 Basic concept

Light-induced cleavage of water into concomitant evolution of H_2 and O_2 is classified as an "up-hill" photoinduced reaction which is largely a result of a high positive change in the Gibbs free energy (+234KJ/mol). Water splitting occurs when photon energy is transformed into chemical fuels. The nature of this reaction has made some experts to dub it as "artificial photosynthesis" as delineated by green plants' photosynthesis. Figure 2.3 shows the typical water splitting in a solid photocatalyst. In the presence of illumination, if photon energy is greater than bandgap of the photocatalyst, the electrons of the valence band are promoted to

the conduction band. The excitation of electrons from the valence band brings about vacant spaces which are termed as holes.

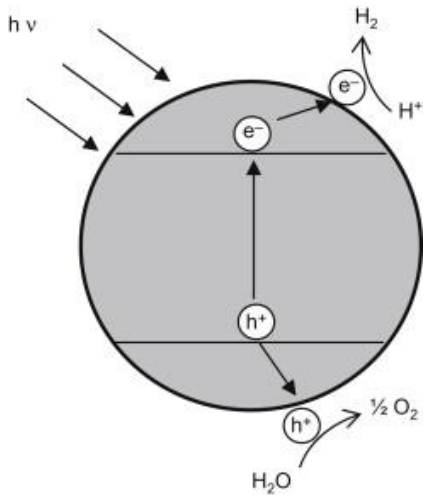

Figure 2.2: A schematic of water splitting effect[109]

Based on existing literature, photocatalysts for water splitting are of two configurations: PEC cells and Particulate systems. The basic PEC cell system for water splitting is designed by the immersion of two electrodes in an electrolyte. One of the electrodes is exposed to light, this is known as the working electrode while the other is called a counter-electrode. However, in particulate systems, the photocatalysts are primarily made up of particles or powder suspended in aqueous solution. Each particle in the particulate system serves as a microphotoelectrode that performs simultaneous oxidation and reduction reactions on its surface. This process does not require the use of a conductive substrate which lends it easily to traditional synthesis pathways. Ultimately, it can be inferred that particulate systems are easier and simpler to fabricate as compared to PEC systems. Nevertheless, particulate systems have their disadvantages when juxtaposed with PEC systems. In terms of charge carrier's separation, particulate systems have lower charge separation efficiency as compared to PEC cells. In the same vein, there are also associated challenges that are tied to the seamless separation of the stoichiometric mixture of oxygen and hydrogen to prevent backward reaction.

The underlying components that make up the performance and overall efficiency of PEC systems are efficiencies of light absorption η_A, charge carriers' separation η_{CS}, charge transport η_{CT} and charge collection/reaction efficiency η_{CR}

Therefore, the efficiency of converting solar radiation into hydrogen fuel, η_{STH} can be evaluated as[110],

$$\eta_{STH} = \eta_A \times \eta_{CS} \times \eta_{CT} \times \eta_{CR} \quad (2.5)$$

Another metric that can be used for the assessment of the PEC performance of photoelectrode is photon-to-current efficiency (η). This is expressed as[111],

$$\eta\,(\%) = \frac{J_{ph}(1.23 - |E_{app} - E_{ocp}|)}{P} \times 100 \quad (2.6)$$

where E_{app} = applied bias, J_{ph} = current generated per unit area (mA/cm^2), E_{ocp} = open circuit voltage when J_{ph} was measured, P = power density of incident light (mW/ cm^2)

STH conversion efficiency significantly varies on the optical and electrical properties of the electrode. These properties are affected by shape, size, and morphology. Nanomaterials that generate hydrogen under visible light irradiation have high quantum efficiency (QE). This can be expressed as[112],

$$QE(\%) = \frac{number\ of\ reacted\ electrons}{number\ of\ incident\ photons} \times 100 \quad (2.7)$$

$$QE(\%) = \frac{number\ of\ evolved\ hydrogen\ molecules}{number\ of\ incident\ photons} \times 100 \quad (2.8)$$

This work however is focused on PEC systems used for simultaneous hydrogen and oxygen evolution systems excluding work on particulate photocatalytic systems which has been reviewed elsewhere[109].

2.3.2 Mechanics of PEC operation

PEC water-splitting systems was first fabricated by Fujishima and Honda in 1972[113]. The mechanics of the reaction is basically in 4 major stages, which are creation of electron–hole pairs after exposing light on the photoelectrode, the oxidation of water by photoinduced holes on the photoelectrode surface to generate H^+ and O_2, the transport of photogenerated electrons to the cathode via an external circuitry and the reduction of proton (H^+) by photoinduced electrons on counter electrode to produce H_2 [113]. The energetic requirements for water splitting are that the real or applied potential must be higher than the minimal potential needed to surmount over-potential and other losses in the system[114].

The general working theory behind PEC water splitting is the transformation of sunlight into hydrogen by applying an external voltage unto the photoelectrode immersed in an aqueous solution which comprises redox couple, one of which is a semiconductor which transforms sunlight into electricity. Electricity (in the form of electron-hole pairs) were then used for water splitting. Based on the exclusive nature of semiconductors to act as a photocatalysts, it performs a crucial role in the activation of redox processes (oxidation and reduction) in the presence of light. These photoanodes can absorb light, which serves as energy source needed to initiate redox reactions. The extra bias needed to make the reaction possible is the externally applied chemical or electric voltage. The external applied voltage makes adequate bias for the PEC system to successfully propel the reaction at a preferred current density by surmounting the slow kinetics. The photoanode generally absorbs photons, and the absorbed photons dislodge electrons thereby allowing for creation of electron-hole pairs necessary for redox processes. As a result, photoinduced electron can reduce H^+ to H_2 while holes can oxidize the water molecule [115–117].

Fermi Energy (E_f) can loosely be defined as the average energy of electrons in a material. However, more technically it is the probability of locating electron halfway in the energy band of materials. It is especially useful when measurements are done in the presence of reference electrode. For intrinsic semiconductor, E_f is usually at the middle of the bandgap (the space between energy at the conduction bandedge (E_C) and valence bandedge (E_V)). The nature of dopant determines how E_f shifts either away or towards the E_C as depicted in Figure 2.4. Equilibrium is attained at the junction by matching the redox couple of electrolytes with the corresponding shift in fermi energy. This is manifested as a veneer thin layer often called depletion layer occurring at the semiconductor surface. This depletion layer is exemplified by the bending of bands downwards or upwards, contingent upon the kind of semiconductor (n-type/p-type) as shown in Figure 2.5 [113]. Optimizing the totality of processes in a single semiconductor component has proven to be an unfeasible feat. Large swathes of efforts have been geared towards improving a broad range of light spectrum together with efficiency. One of the laudable efforts is the design and fabrication of heterostructure photocatalysts (n-n/p-p/ n-p junctions). This has successfully increased the separation and migration of free carriers. At the same time, the annihilation of free carriers in heterojunctions has also been lowered. Based on Figure 2.4 and 2.5 we can summarize that, there is a powerful tendency to increase efficiency of water splitting by improving on the electronic properties of the photoanode[118–120].

Z-scheme is a two-stage process required for PEC water splitting. It involves the imitating of natural photosynthesis. Photoexcitation and a reversible redox process are performed by two distinct semiconductors. A straightforward diagram describing Z-scheme is displayed in Figure 2.5. Z-scheme, in contrast, as more capability to efficiently utilize visible spectrum of solar radiation than conventional one-step process. For this process, the reduction of protons by electrons in the conduction band leads to production of hydrogen. The evolved hydrogen generated electron acceptor which is then transformed to its reduced form. Holes in the valence band also brings about oxidation of donor electron. Thus, the existence of redox pair cycle makes possible water splitting The elements affecting Z-scheme phenomenon are the presence of cocatalyst, electronic and structural features of the photocatalyst [121]. The improvement in the photocatalytic process occurs via the Z-scheme migration of the photoinduced charge carriers [122].

Figure 2.5 (a, b) shows n-type and p-type semiconductors used for PEC water splitting. In Figure 2.5 (c), two distinct photocatalysts are merged, harnessing light energy more efficiently resulting in simultaneous oxidation and reduction reaction. To augment PEC efficiency, annihilation of charge carriers(recombination) must be diminished. The creation of charge carriers happens at the surface of nanomaterials due to increased surface-to-volume ratio occasioned by size on a quantum scale, modulated morphology, and shape. A myriad of studies have disclosed an increase in the efficiency of PEC water splitting in a range of 50%-90% [116].

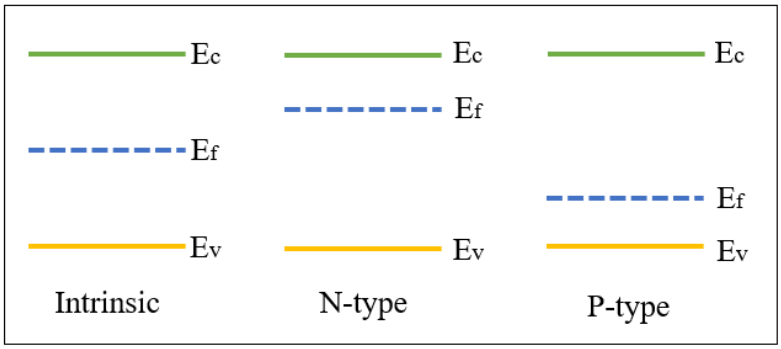

Figure 2.3: Schematics on E_f shift for extrinsic semiconductor

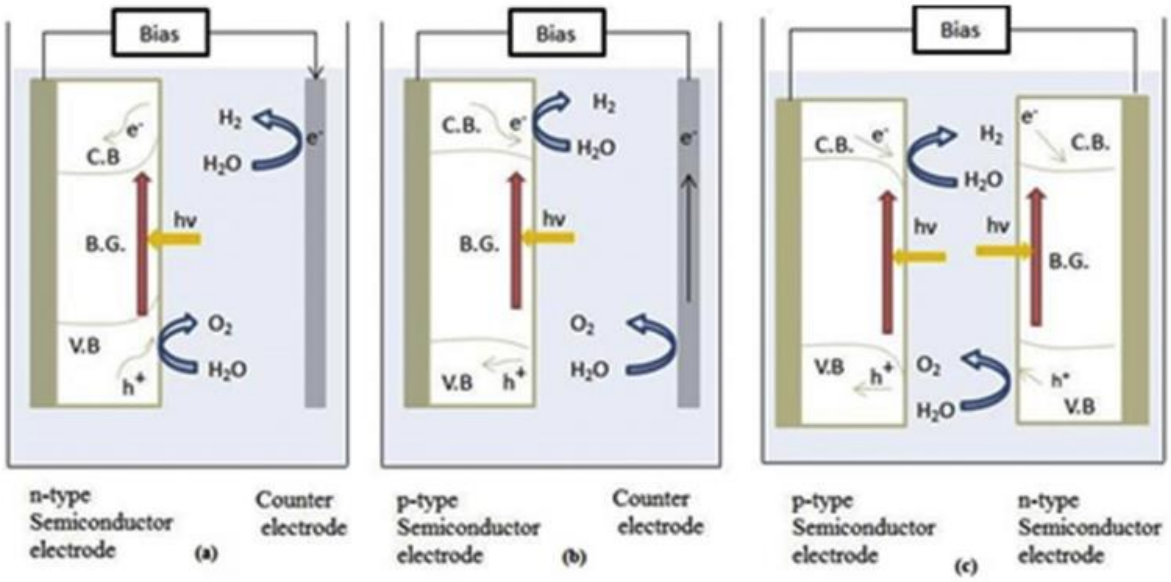

Figure 2.4: Z-scheme of PEC water splitting using n-type and p-type semiconductors[123]

The overall reaction involved in water splitting mechanism [118].

$$2H_2O + hv \longrightarrow 2H_2 + O_2 \; \Delta G^0 = 4.92\text{eV}(113\text{kcalmol}^{-1}) \tag{2.9}$$

$$4H^+ + 4e^- \longrightarrow 2H_2 \; E^0_{red} = 0\,V \tag{2.10}$$

$$2H_2O \longrightarrow 4H^+ + 4e^- + O_2 \; E^0_{red} = 1.23\,V \tag{2.11}$$

2.3.3 Factors Affecting PEC efficiency of nanomaterials.

PEC performance and STH efficiency essentially rely upon morphology, orderliness and uniformity. Apart from the decrease in size, the modulation of the structure and shape are critical in mechanics of water splitting.

1) Temperature and Pressure

The role of temperature in the improvement of PEC efficiency is indispensable. For the most part, high temperatures are needed for most experiments. In one study, low temperature treatments showed an enhanced PEC efficiency. Researchers revealed that, an increase in working pressure increases the band gap of the material [124]. At low temperature, IPCE can rise up to 95% [125].

2) Size

The fabrication of good catalyst is one of the approaches to augment PEC efficiency. By tuning the size of materials appropriately, a gain in the photocurrent response can be achieved. In very

small fine particles, the dominant aspect is electro-kinetics which leads to high charge carrier recombination. For bigger particles, improved charge extraction at the electrode/electrolyte junction can be accomplished due to band bending. In this way, large co- catalysts are suitable for better PEC performance [126].

3) Crystallinity

Well-ordered crystal structures show superior performance when contrasted to amorphous crystals. TiO_2 nanotubes with an ordered degree of arrangement have increased hydrogen evolution via water splitting. The photocurrent density of well-ordered (anodic TiO_2) nanotubes is greater than the typical TiO_2 nanotubes by about a factor of 2.2 and its charge transport is excellent when electrolytes have immediate contact with large internal surface area of the tube[127]. The quality of the crystal has a bearing on the decrease in defect density and thus reduce charge carrier recombination, which shows morphology or structural feature can significantly affect photocurrent efficiency.

4) Light

The source of light must be specified in terms of the spectral distribution. AM1.5G light spectrum power density is measured in power per unit area as 1000 W/m^2 [128]. The addition of dopants to semiconducting nanomaterials allows for the absorption of the UV and visible spectral component of solar light[129]. A range of other factors can also have a significant bearing on photocatalytic activity. For example, semiconductor-semiconductor or semiconductor-metal junction properties, grain morphology induced by processing-route, grain nucleation induced by doping, lattice impurity, desorption and adsorption kinetics dependent on pore structures, exposure of certain facets [130].

5) Bandgap

The primary benefit of semiconductors is the tunability of the bandgap of the materials. The narrowing of the bandgap has the powerful ability of increasing light absorption across a broad range of light spectrum and subsequently the enhancement of PEC properties [131–134]. If the bandgap is large, the photons are inefficiently absorbed to break water molecules because the energy are insufficient to promote energy to the conduction band thereby increase losses due to non-absorption of light. The suitable bandgap for efficient PEC system is the range of 1.6-2.2 eV. For energy within this interval, there is an increase in charge carrier mobility. The

reduction of the bandgap can be accomplished through injecting acceptor or donor materials into the nanomaterials.

6) Dimensionality

Zero, one, two and three dimensional (1D, 2D, 3D and 0D respectively) structures are the major classifications of nanomaterials on the basis of dimensionality. NRs and NWs are more responsive to light and charge carriers' transporter when compared to thin layers. Nanotubes (NTs) have high surface area, which accelerates the rate of redox reaction than NRs and NWs. This is so in spite of the small fraction of the area presented to light.[110]. 1D structure provides a short single defined pathway for free carriers, leading to a reduced destruction of charge carriers(recombination). 3D nanomaterials are also known for high PEC performance. It has increased light absorption by decreasing the pathway for the diffusion of the photoinduced holes across photoelectrode/electrolyte junction [110]. 0D nanostructure, in the same vein, has demonstrated efficient absorption of light and excellent photocatalytic activity. At the point when a semiconductor is modified with quantum dots with appropriate bandgap, this modification allows for a decrease in recombination whilst bringing about high sensitivity to visible portion of solar light [135].

7) pH dependency

pH values significantly impact on PEC system operation. The electrochemical potential of water splitting reaction relies heavily on pH of electrolytic solution, which determines overall charge attracted to surface sites such as negative, positive, and neutral. At the same time, to minimize photocorrosion and enhancing photostability and efficiency, pH of electrolyte would be modulated depending on the nature of anions and electrolyte. The movement of charged species during redox processes can weaken the surface of the photoelectrode. Some photoelectrodes display steadiness in photocurrent response in different pH conditions[136,137] . It has been demonstrated that photoresponse and photostability can be enhanced by buffering the electrolyte[138].

2.3.4 Doping of ZnO for PEC

The most critical component in PEC water splitting devices is the photoelectrode. In this work, ZnO photoelectrode is employed. It is essential for a photoelectrode to meet the following criteria: a good photoelectrode must be very responsive to light, be inert to electrolyte and possess the essential electronic band positions that is in tandem with electrochemical scale so that the electrons and holes would have necessary potential to drive the redox processes.

Following the years of scientific studies, the central technical bottleneck remains the fabrication of photoelectrode structures effectively harness conversion light visible component of solar radiation[139].

In the bid to surmount this challenge and especially in the design of ZnO nanostructures that are sensitive to photons within the visible spectrum, deliberate doping with metals, rare-earth metals, transition metals, non-metals and co-doping approach have all been attempted and well documented in the scientific literatures. This is to ensure enhancement in the absorption of solar irradiation, increase in photoresponse and ultimately the water splitting effect of the material. In this literature review, doping of ZnO for water-splitting application would be split in 2 categories. Doping using non-group V elements and group V elements. The classification is based on the fact that, this study tried to investigate the effect of bismuth—group V element—on the PEC performance of ZnO NRs. This is to give some sort of account on the different dopants that have been successfully used in improving the photocurrent response of ZnO.

2.3.4.1 Doping using non-group V element

Different elements. For example, Iron (Fe), Copper (Cu), Carbon (C), Cerium(Ce), Cobalt (Co) have been effectively used as dopants for investigating PEC performance of ZnO under visible light irradiation. Sol-gel process was used to synthesize Ce-ZnO films at an operating temperature 500 ^{o}C. Under visible light, CA measurement showed that the maximum photocurrent of 1.2 mA/mm^2 was generated at an applied bias at 1.2 V (vs. Ag/AgCl) [140]. A counterstrategy was used to fabricate C-ZnO hierarchically porous nanoarchitectures on indium tin oxide. The photoactivity of C-ZnO nanoarchitecture in water splitting without sacrificial reagents was characterized. This hierarchical structure was juxtaposed with other traditional ZnO photoanodes in reported publications. Analysis showed that C-ZnO has a remarkable photocurrent response. The typical ZnO structures and pristine ZnO hierarchical nanoarchitectures produce photoresponse of 0.02 and 0.77 mA cm^2 at +1.0 V under visible light illumination. In contrast, the regular C-ZnO hierarchical nanoarchitectures have the highest photocurrent pegged at 1 mA cm^2. The re-engineering of the ZnO structure using C as dopant improved the visible light absorption and STH efficiency when compared with traditional ZnO structures. Other metrics were measured in the study such as overall IPCE with a maximum value at 95%. Also, IPCE at a monochromatic wavelength of 400 nm was recorded at 26.6%[141]

A string of 120 materials containing 27 different mole fractions(between 0 and 0.068) was fabricated by automated serial electrochemical deposition. This method was used to study C-doped ZnO films for the evolution of hydrogen using PEC system. Electrochemical characterization processes showed increased hydrogen evolution for Co-doped ZnO films especially with the material doped with 4.4 at.%. The addition of 4.4 at.% Co in ZnO film led to bandgap shrinkage from 3.20 eV to 2.75 eV, increase in photocurrent from 15 $\mu A/cm^2$ to 55 $\mu A/cm^2$ thereby showing an enhancement over pristine ZnO with by a factor of 4 under zero applied voltage[142]. Cu-doped ZnO films were grown on glass substrate using sol-gel solution synthesis method. The optical characterization of the doped sample depicted two dominant peaks for wavelengths in the UV. One has a slightly greater energy while the second has a bandgap that corresponds to bulk ZnO indicating quantum confinement in Cu-ZnO films. The doping of copper affects the two bandgaps distinctively. The addition of Cu 1 at.% into ZnO film that is thermally annealed at 600 °C leads to a 141% improvement in photoresponse at no external bias[143]

Fe-incorporated ZnO NRs were grown on ITO substrates at low temperature via electrochemical method. The injection of Fe dopant from 0 to 4 at. %, causes a change in band gap from 3.26 to 3.28 eV, the increase in bandgap energy has been credited to Burstein-Moss effect. Not only does the bandgap increase, but there was also an increase carrier concentration in Fe-ZnO thin films ranging from 2.81×10^{18} to 4.29×10^{18} cm^{-3} as composition of Fe increase between 0 and 2 at.%. The existence of Fe dopant nanostructured films has an effect on photovoltaic properties of the materials as typified electronic disorder and photocatalytic activity. The PEC characterization methods revealed under UV light, significant photocurrents were produced for Fe-ZnO nanomaterial. Tauc plots was used to compute the bandgap of the materials, analysis of the results showed a slight change in bandgap with the addition of Fe with values within the interval 3.26 and 3.28eV which is in consonance with established literature[144]. $AlCl_3$ as the dopant precursor was used to obtain Cl-doped ZnO NWs. Photocurrent measurement showed that at zero applied voltage, photoresponse of the Cl-ZnO NW was 2.0 mA/cm^2, this corresponds to value that is 2 times higher than pure ZnO NW. Optical characterization also showed that there is similarity in light absorption between pure and Cl-doped ZnO. Nevertheless, this increased photoresponse due to Cl doping can be linked to the increase of the conductivity charge carrier in ZnO NWs, which has brought about charge carrier collection efficiency and reduced recombination[145].

2.3.4.2 Doping using group V element

The default product for doped ZnO material including group V-based ZnO is n-type in nature. However, the essential ingredient needed to widen ZnO applications in optoelectronic applications is the skilful modulation of p-type and n-type electronic doping [146]. Several efforts have been spent by academic researchers on this path for decades. Based on theoretical predictions, it is believed that group V elements are acceptor materials and that the major hindrance towards producing stable p-type semiconducting materials is the high activation energies of this materials. Although, significant number of experimental works have shown that N, P, As, Sb and Bi can produce the stable and low-resistance p-type ZnO and thereby disproving the claims of the theoreticians[147–151]. The mechanics behind the p-type nature of ZnO caused by group V elements remains a subject of debate.

Even though, group V-based p-type ZnO can be achieved with impressive reproducibility in the laboratory. There has been little, or no research work specifically targeted at PEC water splitting. Perhaps this could be a result of the fact that n-type ZnO has a higher conductivity than p-type owing to higher conductivity of electrons than holes. In retrospection, most of the research have focused more on N-doped ZnO nanostructures.

Yang *et al.* reported a significant increase in PEC performance of ZnO NRs upon incorporation of 4 at% of N: Zn. At +1.0 V, there is an increase in photocurrent from 17 $\mu A/cm^2$ to 400 $\mu A/cm^2$. The increase in photocurrent upon nitrogen addition was attributed to the sensitivity of the material to visible frequencies of the solar spectrum as supported by the UV-vis data[152].

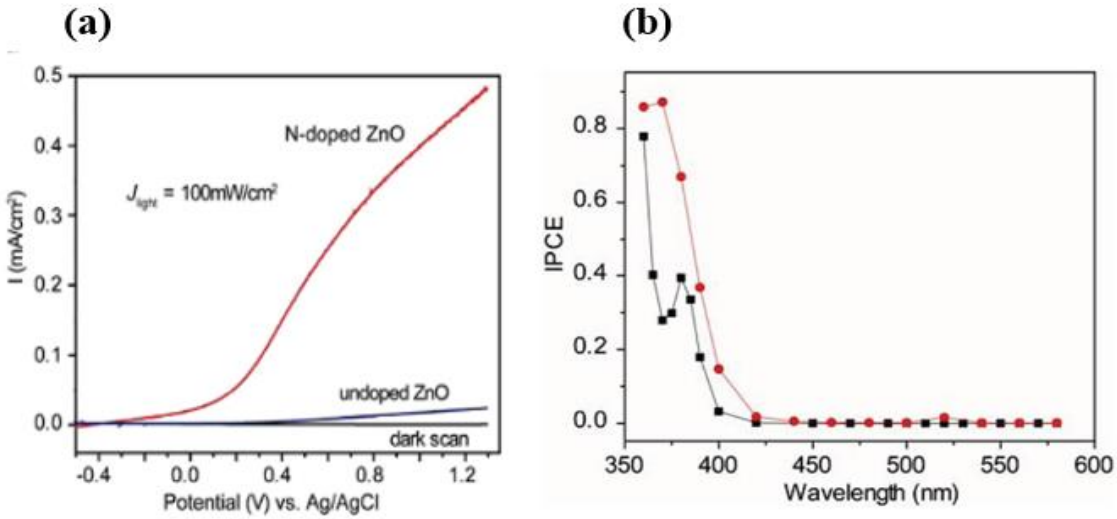

Figure 2.5: (a) LSV data of undoped ZnO NWs and N:ZnO NWs at scan potentials -0.5 to +1.3V (b) Measured IPCE spectra showing 3.7% gain in efficiency between 360-580nm. Undoped ZnO NWs (black line), N: ZnO NWs (red line)

Reactive radio frequency magnetron sputtering was used to synthesize N-doped ZnO films. The doped material was characterized and its photoresponse compared to pristine ZnO films. Tauc plot revealed that doping with nitrogen caused a redshift in the peak of light absorption indicating visible light absorption resulting from reduced bandgap of ZnO films. Additional analysis also showed ZnO:N films displayed a significant increase in photonic absorption in high-energy region with wavelength on the order of 600 nm. Therefore, under visible light, ZnO:N films exhibit higher PEC performance than pristine ZnO [153].

The general observations extracted from conventional doping of metal oxide photocatalysts present an unfortunate condition. This involves the recombination of significant amount of free charge carriers created via visible light excitations before being transported to the appropriate sites (counter electrode and photocatalysts surface) where they react electrochemically to form hydrogen and oxygen evolution reaction. With the recognition of low photocurrent challenge, some strategies have been tried to increase the conversion efficiencies of photoelectrodes that are based doped metal-oxide — of which one of them is co-doping. Co-doping has proven potent in the passivation of the traps at the bulk and surface of the materials with improved efficiency of photo response and water splitting.

Combustion synthesis method was used for preparing co-doped ZnO samples containing cadmium and indium using chloride precursors. He concluded that photoelectrochemical response of the co-doped samples improved relative to the pristine ZnO over range of wavelength between 300 and 450nm[154]. Radio-frequency magnetron sputtering was used to fabricate co-doped ZnO films containing Al and N, (Al, N)-ZnO. The as-synthesized samples were performed in a gas environment comprising blended N_2 and Ar and blended N_2 and O_2 at 100^oC. It was observed that nitrogen was better incorporated in the ZnO films in the N_2 and O_2 gas environment Thereafter, PEC performance was investigated, the results showed first that gas ambient is crucial for proper incorporation of dopants into the crystal lattice and that (Al, N)-ZnO co-doped samples is sensitive to light in the visible spectrum[155].

Shet *et al.* investigated co-doped ZnO films containing Ga and N, (Ga, N)-ZnO and its photocurrent response. Upon preparation of co-doped samples, post-annealing was performed for 2 h at an operating temperature of 500 °C in air. PEC results showed that co-doping using Ga and N enhanced crystallinity and reduced bandgap with a concomitant effect of high absorption over the visible spectrum with a maximum photocurrent recorded as 100 mA/cm^2 with an applied bias at 0.8 V (vs Ag/AgCl) [156].

A comprehensive research into the effect of group V dopants on the PEC water splitting revealed little or no documented literatures on P, As, Sb and Bi-doped ZnO on the PEC water splitting. More so, a thorough search launched on the use of bismuth dopants on ZnO and its PEC performance revealed that perhaps there is no existing literature on this topic. The reason for this was explained quite succinctly by Abed *et al.* who reported that bismuth doping of ZnO is a rare practice which could be ascribed to the segregation of the bismuth when incorporated into the ZnO lattice[17]. The addition of bismuth to ZnO film using pulse laser deposition has been reported to be adversely affected by phase separation of β-tetragonal Bi_2O_3 and ZnO bringing about high resistivities making it difficult to control the conductivity of ZnO. The study concluded that low doping concentration is crucial to study behaviour of bismuth doping.[157]. In the aftermath of this study, a report showed that the synthesis of Bi-doped ZnO films was possible without phase separation by maintaining a concentration of bismuth below 0.4% even though room-temperature hall effect measurements displayed a significant decrease in electron concentration and an increase in resistivity for Bi-doped ZnO films[158]. In contrast with the studies above mired with the either phase separation or conductivity issue, a later study realised low-resistivity and stable p-type Bi-doped ZnO using pulse laser deposition under rich oxygen atmosphere and post-annealing conditions[151].

In sum, it can be affirmed that group V elements have been successfully used to improve the optoelectronic properties of ZnO using physical and chemical vapour deposition methods as discussed above with very few reports on solution-process approach like hydrothermal (a gap this study tries to fill up). More so, the dopants have been incorporated into the ZnO lattice using approaches such as ion implantation that involve addition of dopants onto the surface of ZnO material thereby passivating the dangling bonds with a result of reduced surface recombination while at the same time avoiding bulk recombination that comes with creation of defects within ZnO nanostructure.

2.3.5 Photostability of ZnO

The perfect semiconductor electrode used for water splitting would require a certain set of criteria: (I) a reasonable bandgap width >1.23 eV (which needs +0.8 eV to surmount kinetic bottlenecks) (II) the conduction band over the $H+/H_2$ balance potential for hydrogen production and the valence band underneath the O_2/H_2O balance potential for oxygen production [128,159]. As of late, nanostructure redesigning of ZnO films has appeared to increase photocurrent yields due to monumental surface-to-volume proportion, which imparts incredible property to nanomaterials, leading to efficient delivery of charge carriers and thereby enhancing PEC performance. Notwithstanding these amazing properties, ZnO-based photoanodes are not marketable to help dependable and efficient photoactivity in the light of a few shortcomings. Most remarkably, ZnO experiences chemical dissolution in the electrolytes under ultraviolet irradiation due to the trapping of holes on its surface, which is a typical issue for a host of other applicable materials for water splitting. Gerischer contrived the thermodynamic and kinetic conditions that are necessary for controlling the photodecomposition of semiconductors and it also showed the situations when photodecompositions can be avoided after the application of these conditions to a limited semiconductors[18]. In brief, electrons can secure a semiconductor from photodecomposition if its photodecomposition potential (E_{DCe}^{-}) is negative(a potential just below the conduction bandedge). In the same vein, holes can protect semiconductors from decomposition if its photodecomposition potential (E_{DCh}^{+}) is positive(potential above the valence bandedge). This standard situation is depicted in Figure 2.7(a). ZnO is steady against photodecomposition by electrons but is fundamentally unstable to photodecomposition by holes, as shown in Figure 2.7(b) [138]

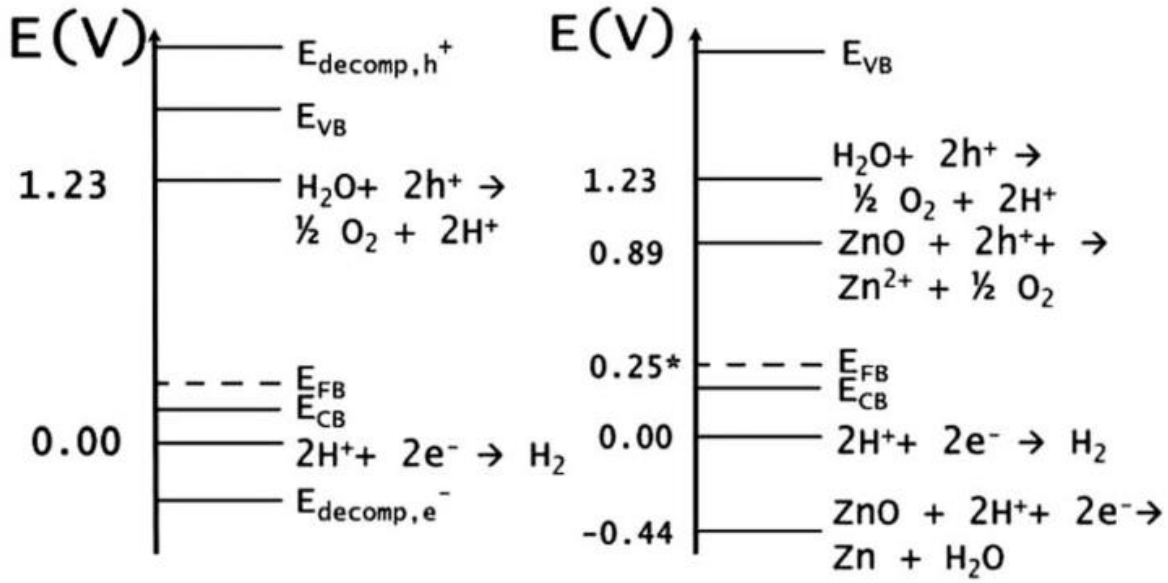

*Figure 2.6: (a) Energy band diagram for a perfect stable n-type semiconductor at zero pH (b) Energy band diagram of ZnO zero pH. E_{FB}, marked with *, was recorded based on computations*[138]

The decomposition potential is a function of the dissolved products precipitated when the working electrode corrodes [160]. It is noteworthy to mention that chemical dissolution can be prevented when water is oxidized at a potential that is lower than E_{DCh}^+. In the light of this, the relative positions of the potentials relating to the contending reactions need to be decided over the available pH range. It is notable that the redox potential of the 1/2 O_2/H_2O couple with rising pH has potential/pH value of ~59 mV/pH [161]. The E_{DCh}^+ of semiconducting oxides is largely neutral to pH, but this is invalidated in the face of ZnO[162]. A constant decomposition potential in the entire pH gamut would be feasible if the product generated at any pH solution remain consistent. ZnO decomposition when the solution pH values are too low or too high, even in dark. The potential/PH diagram of ZnO reveals that at pH ranging from acidic to neutral, pH 9.2–13.2 , and at exceptionally high alkaline pH, the prevalent dissolved zinc species are Zn^{2+} , $HZnO_2^-$, ZnO_2^{2-} respectively [163]. Dissolution of ZnO in electrolyte has been suggested as the subsequent reactions below.

$$ZnO_{(s)} + 2H^+ \longrightarrow Zn^{2+} + H_2O \quad (2.12)$$

$$ZnO_{(s)} + H^+ \longrightarrow ZnOH^+ \quad (2.13)$$

$$ZnO_{(s)} + OH^- + H_2O \longrightarrow Zn(OH)_3^- \quad (2.14)$$

$$ZnO_{(s)} + 2OH^- + H_2O \longrightarrow Zn(OH)_4^{2-} \quad (2.15)$$

The dissolution process is a result of the complex interplay of reaction protons and hydroxyl ions and ZnO[164]. The destructive reaction of ZnO normally needs potential applied at around 2 V (vs SHE). [165]. Accordingly, two contending reactive processes for ZnO disintegration were proposed [166]

$$2ZnO \longrightarrow 2Zn^{2+} + O_2 + 4e^- \quad (2.16)$$

$$ZnO + 2H^+ \longrightarrow ZnOH^+ + H^+ \longrightarrow Zn^{2+} + H_2O \quad (2.17)$$

Although, the dissolution kinetics of ZnO is progressing sharply under irradiation than under applied bias. This is perhaps a result of the dependence of the process on the concentration of OH^-. As a matter of fact, the dissolution rate of ZnO is dependent on hole concentrations and OH^- at the surface of ZnO. The concentration of this chemical species are also dependent on both light intensity and applied voltage[167]. The chemical equations illustrating the light-induced deterioration of ZnO are stated as follows[168]

$$ZnO + 2p^+ \longrightarrow Zn^{2+} + \frac{1}{2}O_2 \quad (2.18)$$

$$ZnO + 3OH^- + 2p^+ \longrightarrow HZnO_2^- + \frac{1}{2}O_2 + H_2O \quad (2.19)$$

$$ZnO + 4OH^- + 2p^+ \longrightarrow ZnO_2^{2-} + \frac{1}{2}O_2 + 2H_2O \quad (2.20)$$

Appropriately, the lowest level of ZnO dissolution is attained at pH 9.3 (10^{-7} to 10^{-8} M) [169] and the ZnO deterioration worsens dramatically when pH becomes greater or smaller than 9.3. Moreover, It has been recommended that rate of ZnO dissolution varies on the nature of anion in the electrolyte, which is proportional to the square root of rotation speed of electrode ─ this can be related to the transport of protons[170].

To surmount the issue of chemical dissolution, two distinct paths are commonly utilized: 1) advancement of strategies to enhance the stability of ZnO for the long-term usage in water splitting; and 2) layers of conductive and protecting films to avert corrosion during the PEC reaction period[171]. In recent times, surface modulation of ZnO photoanodes, for example, coupling with other semiconductor[172,173], addition of noble metals via deposition[174], and sandwiching with carbon [175], have all been suggested to mitigate photocorrosion to provide the long-term performance of ZnO electrodes for the water splitting process. In addition, the

use of electrolytes such as potassium hydroxide (KOH), Na_2SO_4, phosphate, borate and CB have proven effective at augmenting the rate of oxygen evolution whilst maintaining stability.

Fekete *et al*. investigated optimization of electrolytic solution to preserve stability of ZnO photoanodes on a long-term basis. It was asserted that screen-printed ZnO films displayed the highest stability in a borate buffer(pH 10.5). Accordingly, 75% of the original photocurrent was maintained after 12 h, lifetime of the ZnO films increased from approximately 2 h at neutral pH to beyond 12 h in slightly basic buffered pH demonstrating that the lifetime of the photoanode could be increased by a significant factor in comparison to standard testing conditions[138]. Liu *et al*. also reported the role buffered electrolytes have on ZnO NR prepared by hydrothermal method. It was proven that ZnO NR has a significantly high photoactivity and photostability in borate and CB solutions(both have a pH 10.5), the photoresponse generated is greater than 99% of the original value has been preserved after 1 h polarization at 1.5 V (vs RHE) under AM 1.5G. The study concluded with an astonishing discovery which showed that lifetime of ZnO photoanodes can be monumentally prolonged by an order of magnitude in the binary electrolyte comprising borate and carbonate ions. The PEC stability in binary electrolyte outperforms in the distinct and separate electrolytes(borate and carbonate) when used individually; this improvement has been ascribed to the protective behavior of this materials on ZnO NR[176].

Chapter 3 Materials and methodology

3.1 Materials

Zinc acetate dihydrate (Sigma-Aldrich), Zinc nitrate hexahydrate (Sigma-Aldrich), Diethanolamine (Sigma-Aldrich), Bismuth (III) nitrate pentahydrate (Sigma-Aldrich), Hexamethylenetetramine (Sigma-Aldrich), Ethanol (J.T.Baker), De-ionised water, FTO glass substrate (Ossila), sodium carbonate, sodium bicarbonate, sulphate solution.

3.2 Methodology

The purpose of this study is to improve the photoresponse and photostability of ZnO NR by employing the following approach: studying the effect of bismuth concentration and growth time on light absorbance and photoresponse; studying the influence of electrolyte on photoresponse and photostability.

3.2.1 Fabrication protocol

To synthesize materials for this project, fabrication procedures were in 2 stages as delineated below:

Stage 1: Synthesis of ZnO doped with varying bismuth concentration and growth time

FTO glasses (1cm×1cm) were cut in shape and sequentially cleaned ultrasonically in acetone, iso-propyl alcohol (IPA) and deionized (DI) water for 10 min each. The cleaned FTO glasses were then placed in ozone cleaner to dry and remove the residual organic salts. 0.01 M seed solution was prepared by dissolving 0.022 g of zinc acetate [$Zn(CH_3COO)_2 \cdot 2H_2O$] in 10 ml ethanol. The seed solution was deposited via spin-coating onto the FTO substrate and then baked sequentially in ambient air at 100 °C and 50 °C for 15 min and 10 min. The process of spin-coating and sequential baking steps was performed 6 times (to aid vertical alignment of the ZnO NRs) followed by annealing of seed-layered FTO at 300 °C for 1 h. The fabrication of samples was conducted in two-fold, synthesizing pristine and a range of 2-4%wt of bismuth doped ZnO NRs for 2 h and synthesis of pristine and 2%wt of bismuth doped ZnO NRs at 45 min and 2 h growth time. Pristine and bismuth doped ZnO NRs array were prepared by hydrothermal process using equimolar aqueous solution containing 0.04 M zinc nitrate hexahydrate [$Zn(NO_3)_2 \cdot 6H_2O$] and hexamethylenetetramine (HMTA) [$(CH_2)_6N_4$] at operating conditions(90 °C and (45 min and 2 h))**.** Slight modification was made to the bismuth doped samples specifically through addition of bismuth nitrate pentahydrate[$Bi(NO_3)_2 \cdot 5H_2O$] with sample proportions of 2-4%wt of zinc nitrate in the growth solution[177].

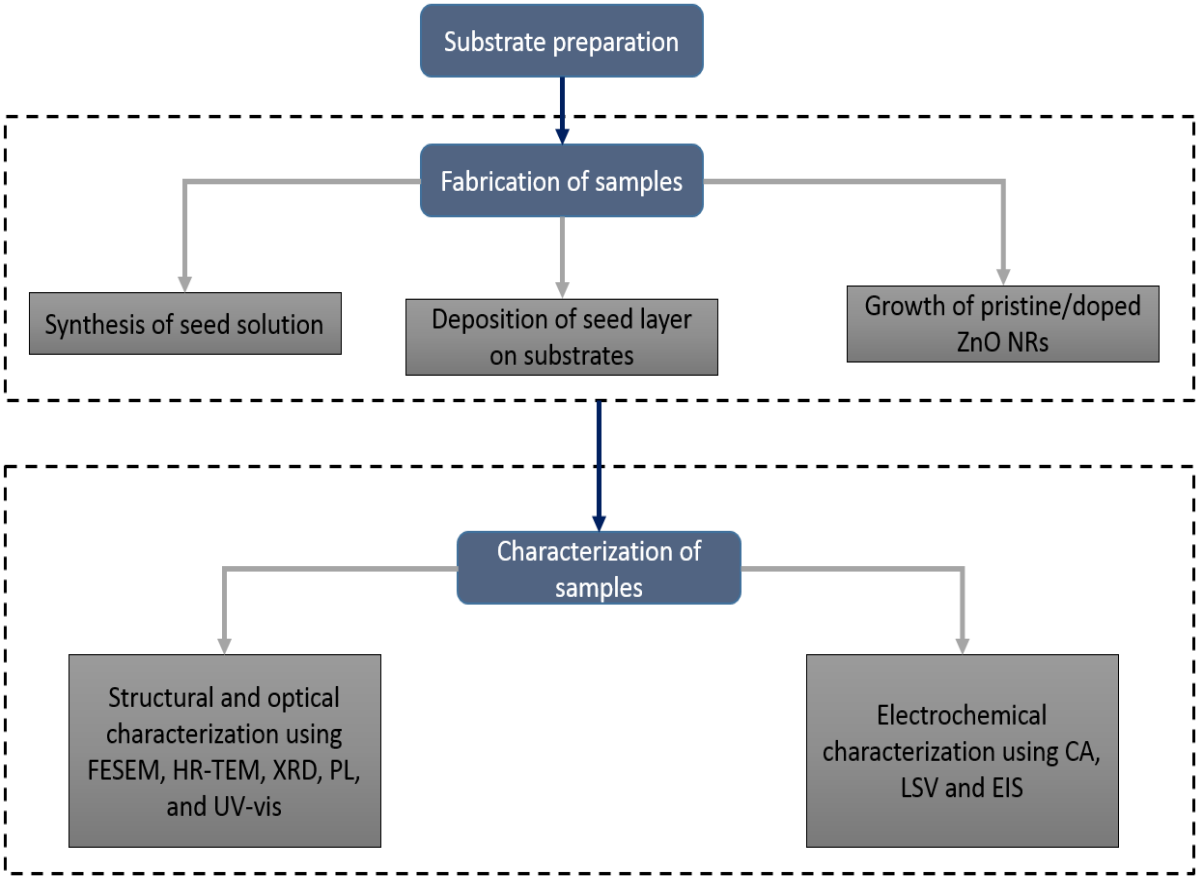

Figure 3.1: Workflow of the fabrication and characterization of ZnO NRs

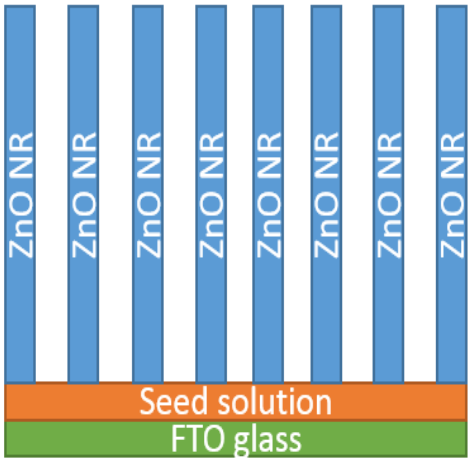

Figure 3.2: Architecture of ZnO NR

Stage 2: Synthesis of electrolytes

0.025M of Na_2SO_4 (Sulphate) solution was prepared by dissolving 0.355g of solute in 100ml water. Also, 0.025M CB (pH 10.5) was prepared by adding 0.038g sodium bicarbonate and

0.217g sodium carbonate in 100 ml water. The two solutions were employed in studying how electrolyte affects photostability of ZnO NR.

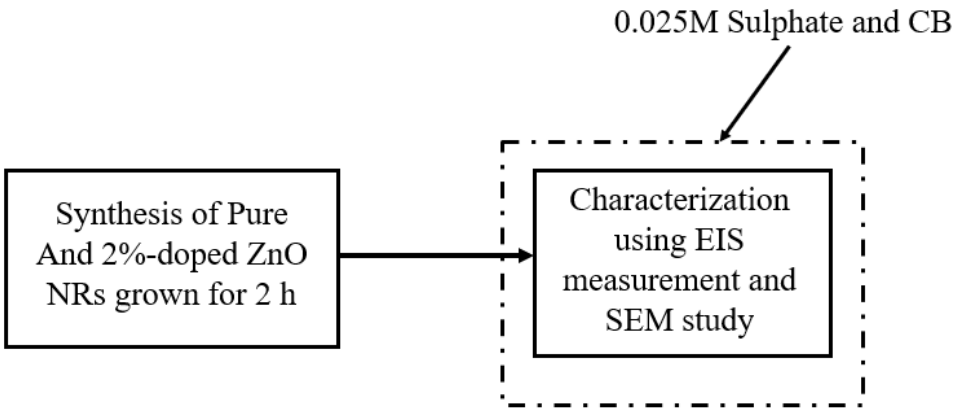

Figure 3.3: Flowchart of the experiment used for studying the effect of electrolyte on photoactivity and photostability of ZnO NR

3.2.2 Structural and optical characterization

The morphology and elemental composition of the as-synthesized materials were studied using field emission electron microscope (FESEM Hitachi SU8010) and energy dispersive x-ray spectrophotometer (EDX) respectively. The crystallography (crystal structure, quality and orientations) of the samples was characterized using XRD (Bruker D8 discover) with CuKα radiation. XRD was used to obtain bragg diffraction peaks of the samples 2θ ranges from 20^{o} to 80^{o} at a scan rate of 0.02^{o} per step and scan size of 0.02^{o} min^{-1}.The density of defect states of the samples was studied using Photoluminescence (PL LabRAM Horiba Scientific) with an excitation wavelength of 325nm. Optical absorption spectra were obtained using UV-vis spectrophotometer (Cary Instruments) in the wavelength range between 350 nm to 700 nm. The absorbance spectra obtained was manipulated using Tauc method to compute bandgap of the samples.

3.2.3 Electrochemical characterization

The fabricated samples (photoanodes) were prepared for electrochemical characterization by securing a copper wire on the exposed conductive part of the FTO with a silver conducting paste. The conductive part was exposed by using HCl and ethanol to remove ZnO NRs on the edge of the FTO surface. The substrate was subsequently sealed on all sides with epoxy resin except the active working area. PEC measurements were performed in a three-electrode mode

with FTO-based ZnO NRs array as the working electrode, a platinum(Pt) rod as counter electrode and a Ag/AgCl reference electrode.

Sequel to stage 1 synthesis route, 0.5 M Na_2SO_4 aqueous solution was used as the electrolyte. Electrochemical measurements were performed on an electrochemical workstation (CH instrument) using chronoamperometry (CA), linear sweep voltammetry (LSV) and electrochemical impedance spectroscopy (EIS). All photoanodes were illuminated from the front side under AM1.5G, UV and Visible (>420nm) illumination provided by simulated halogen lamp (CHF-XM-500W).

Sequel to stage 2 synthesis route, the influence of electrolyte on the as-synthesized samples was investigated via photocurrent measurement and photostability tests. The photocurrent of the materials was collected using Chronoamperometry (CA) measurement under AM1.5G for 3 min and 1 h. The electrochemical phenomena were assessed by fitting equivalent circuits to Electrochemical Impedance Spectroscopy (EIS) measurements.

Chapter 4 Results and discussions

This section is in 3-fold: The first and second part of this section have to do with how bismuth concentration and growth time have an impact on light absorption and photoresponse of ZnO NR thereby highlighting the change in the properties of the materials as a result of change in this growth parameters. Lastly, the use of carbonated buffer and sulphate solution was used to study the impact the photoactivity and photostability on some selected ZnO NR (doped and undoped).

4.1 Analysis of effect of bismuth doping on ZnO NR grown for 2 h

4.1.1 Structural analysis

Figure 4.1 (a)-(d) details the morphology of a pristine ZnO NR and Bi-ZnO NR array. The micrographs show the protrusion of rod like structure from the surface of the FTO substrate. Figure 4.1 (a) indicates that ZnO NRs surface is hexagonally symmetric typifying a wurtzite—thermodynamically stable form of ZnO nanostructures. As the bismuth concentration increases, there is a shrinkage in the mean diameter from 43 nm to 25 nm. In spite of increase in bismuth concentration, average length of the rods is approximately the same with length distribution between 900 nm and 1500 nm. Another interesting fact extracted from Figure 4.1 (b)-(d) suggests the injection of bismuth dopants leads to uneven distribution of the hexagonal facet along the length of ZnO NRs bringing about a conical geometry—with the diameter increasing top-down. It can therefore be inferred that as the rods get thinner with bismuth concentration, the average density of the rods would increase. Figure 4.1 (e) shows the vertical alignment of rods from the substrate surface invariably denoting the deposition of quality seed layers. This is essential for its suitability for optoelectronic applications. XRD spectra in Figure 4.1 (f) shows the presence of FTO substrate, pristine and bismuth doped ZnO NRs. The reflection planes of the FTO have diffraction peaks indexed at 26.43^{o}, 31.91^{o}, 37.87^{o}, 51.59^{o}, 61.6^{o}, while that of crystal planes (100), (002), (101), (102), (103), (112) have bragg's peak indexed at 33.77^{o}, 34.51^{o}, 36. 27^{o}, 47.59^{o}, 62.97^{o}, 65.66^{o}. The predominant bragg's peak observed at 34.51^{o} corresponds to (002) plane implying the vertical alignment of pristine ZnO NRs and Bi-doped ZnO NRs. Interestingly, a 2% increase in the concentration of bismuth increases the intensity of ZnO (002) diffraction peak albeit there is a decrease in the intensity of (002) peak as the concentration of bismuth increase relative to 2% concentration. Hence, Bi(2%)-ZnO NRs has the most vertically aligned ZnO NRs. For bismuth concentration beyond 2%, the reduced (002) peak is followed with an increased number and intensity of reflection planes thereby suggesting more randomness in the arrangement of crystal on FTO substrate.

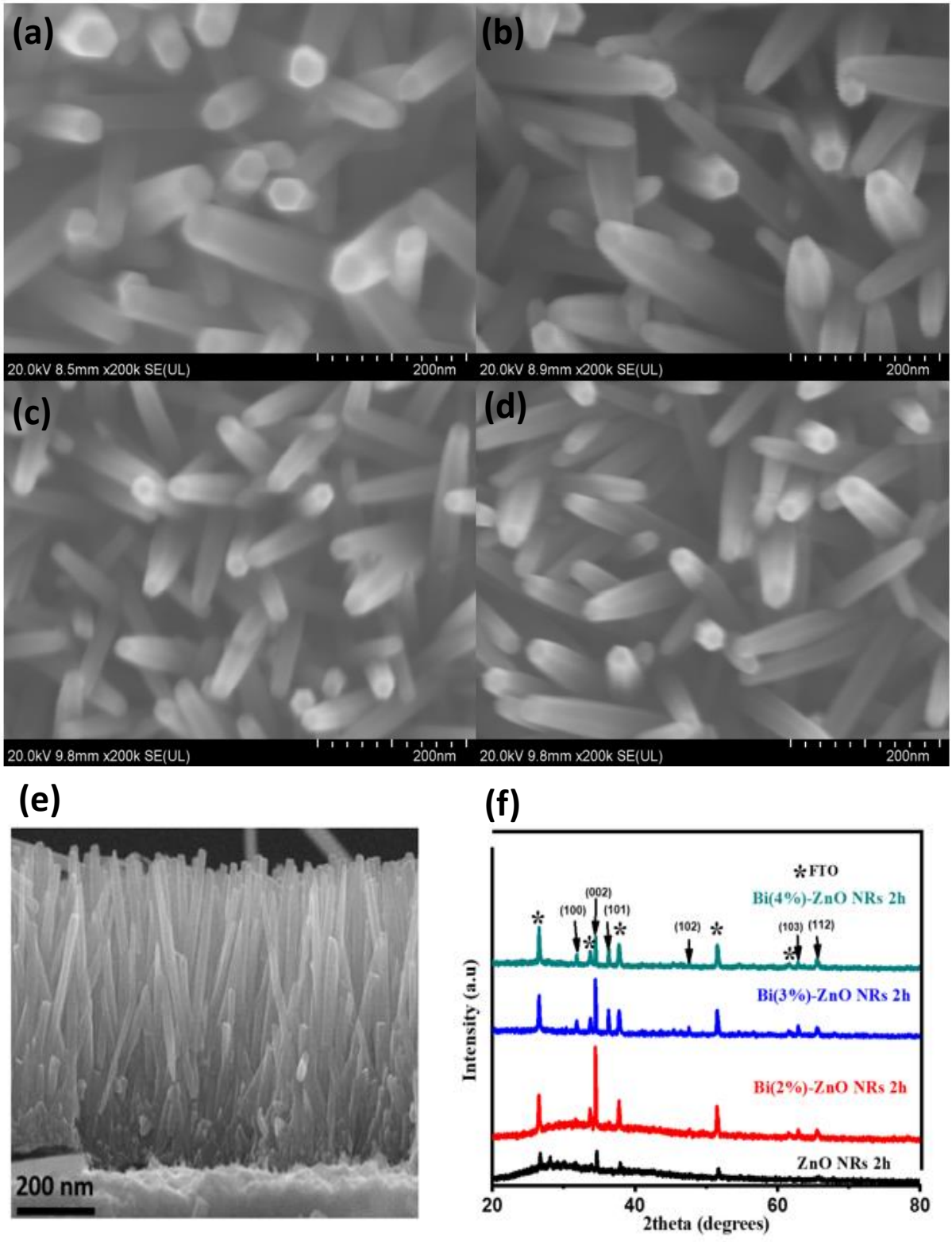

Figure 4.1: FESEM images of Bi-ZnO NR (a) Bi(0wt%) (b) Bi(2wt%) (c) Bi(3wt%) (d) Bi(4wt%) (e) Cross-sectional view of vertically aligned ZnO NRs (f) XRD spectra of Bi(0, 2, 3, 4)-ZnO NRs

4.1.2 Optical and luminescence analysis

Figure 4.2 (a) shows the optical absorption of pristine and Bi(2-4%wt)-ZnO NRs grown for 2 h. Firstly, All Bi-ZnO NRs showed similar spectra with that of ZnO NRs. Bi(2%)-ZnO NRs have the highest absorption within the visible spectrum. The near-band absorption of the as-synthesized materials are collectively approximated at 370 nm with Bi(2%)-ZnO NRs having the highest absorption for wavelength less than 600 nm. Figure 4.2 (b) displays the photoluminescence of as-prepared samples for 2 h.

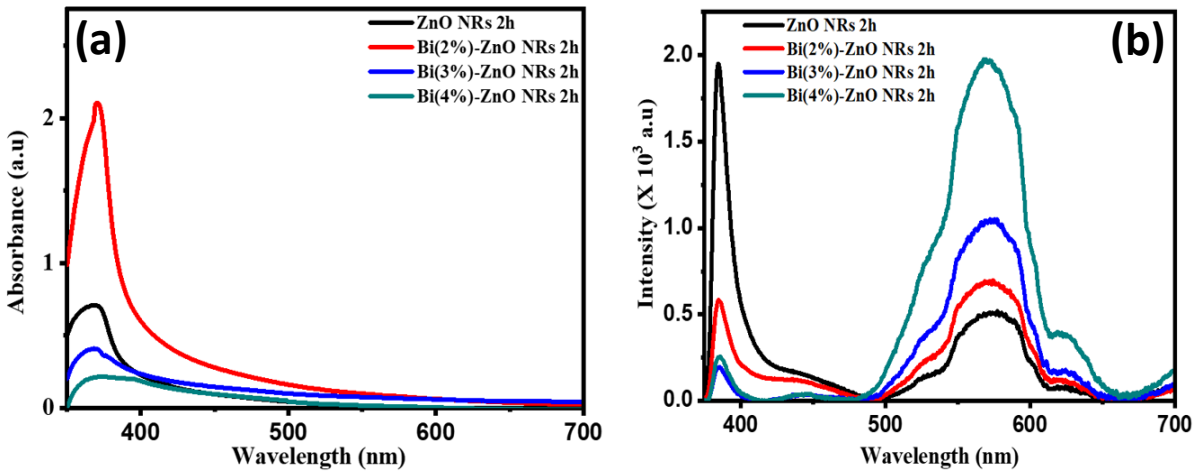

Figure 4.2: (a) UV-vis spectra of Bi(0, 2, 3, 4 wt%)-ZnO NRs (b) Photoluminescence spectra of Bi(0-4%wt)-ZnO NRs obtained using an excitation wavelength of 325nm

PL spectra exhibit UV emission peak at 385 nm for all samples, a blue luminescence between 415 nm and 460 nm, a green-yellow luminescence between 525 nm and 590 nm and orange-red luminescence between 615nm and 700nm. The UV emission peak could be a result of band-to-band transition or donor-acceptor transition[178], blue and green yellow luminescence could be ascribed to interstitial zinc and oxygen vacancies [179–181], and orange-red emission could be attributed to the presence of excess oxygen sites and native point defects[182]. Two major changes were observed with the increase in bismuth concentration. Firstly, luminescent intensity increases due to bismuth-induced defects within the visible range—this is perhaps because introduction of bismuth dopants would create inter-band sites for radiative recombination of carriers leading to wide range emission of different colour light. Secondly, the UV emission peak decreases with increasing bismuth concentration. As bismuth doping levels increase, the bandgap of ZnO NRs decreases as shown in Figure A.1 (a)-(d) confirming successful addition of bismuth.

4.1.3 PEC performance analysis

Figure 4.3 (a)-(e) show that PEC performance of pristine and bismuth doped ZnO NRs was characterised using CA measurements recorded under AM1.5G, UV and >420 nm white light. LSV and EIS measurements were carried out under AM1.5G. The influence of bismuth doping was investigated on the photocurrent of the materials. To study the effect of doping, under >420nm light, Bi(2%)-ZnO NRs has the highest photocurrent with a value of 3.95 $\mu A/cm^{-2}$. This could be a result of a host of factors such as increased light absorption within the visible spectrum due to enhanced inter-band steps created by bismuth dopants as supported by PL data and the predominance of the vertical alignment of the material along the (002) plane. Under UV light, pristine ZnO NRs has the most photocurrent because generally it is a wide bandgap material and responds primarily to UV light. It has been posited that UV photoresponse is positively correlated with mean size of ZnO NRs[183]. Morphological analysis has revealed that bismuth impurities lead to reduction of size of ZnO NRs. Therefore, ZnO NRs performed best under UV illumination because it has the highest mean diameter. Under AM1.5G, Bi(2%)-ZnO NRs performed best because it has the most absorption of light, a defined pathway for ferrying charge carriers with minimal resistance reflective of its vertical orientation. The result is supported by LSV and EIS data recorded under AM1.5G. LSV curves revealed Bi(2%)-ZnO NRs having the highest photocurrent within the range of +0.1 V to +0.6 V while EIS showed Bi(2%)-ZnO NRs with the smallest arc depicting the least resistance at the photoanode/electrolyte interface and thereby supposedly leading to a better charge carrier separation and invariably producing highest photocurrent in AM1.5G as shown by Figure 4.3 (a). Hence, even though the bandgap of Bi(3%)-ZnO NRs and Bi(4%)-ZnO NRs are lower than Bi(2%)-ZnO NRs, they have demonstrably lower photocurrent which can be attributed to higher recombination due to increased dopant concentration.

4.2 Comparison of Bi(0, 2%)-ZnO NRs based on growth time(45 min and 2 h)

4.2.1 Optical analysis

In the case of absorbance spectra for ZnO NRs and Bi(2%)-ZnO NRs as shown in Figure 4.4, the materials with a growth time of 45 min have an absorption of light less than 376 nm while those grown at 2 h have optical absorption between 350 nm and 700 nm. It can be said that as growth time increases, there is an increase in the light absorption across a gamut of photonic wavelength (UV to visible). This may be attributed to an improved scattering of photons due to increase in characteristic length of the materials with growth time[104,183]. For 45 min growth, the incorporation of 2% bismuth concentration increases near-band absorption while

for 2 h growth, there is simultaneous increase in near-band and visible light absorption. With regards to the enhanced visible light absorption, Bi(2%)-ZnO NRs (2 h) do have the highest absorption across the entire range of wavelengths due to the concomitant effect of 2% bismuth addition(which sensitizes visible spectrum of light conceivably a result of the creation of intermediate band steps) and longer length. Figure A.2 shows the tauc plot of Bi(0, 2%)-ZnO NRs grown for 45 min. Using tauc method to estimate the bandgap of the materials, it was deduced that regardless of the doping level of ZnO NRs, the bandgap reduces with growth time—this might be a product of increased density of bismuth-induced defects arising from the increased length with time.

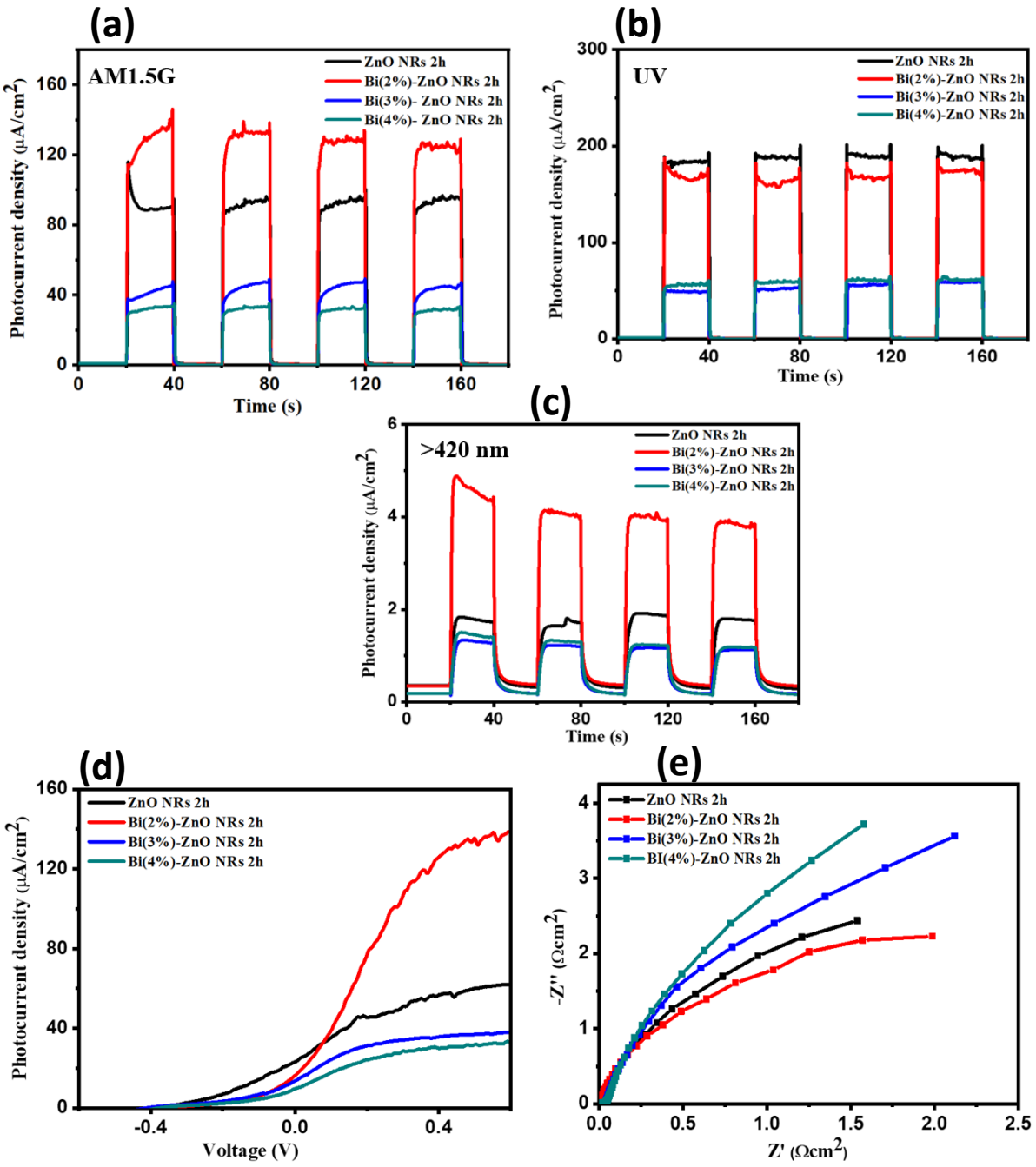

Figure 4.3: (a)-(c) CA plots of Bi(0, 2 , 3, 4%)-ZnO NRs photoanodes collected at applied voltage of +0.4 V under AM1.5G, UV and Visible(>420nm) light respectively (d) LSV plot recorded with a scan rate of 0.1 V/s and applied voltage ranging from -0.6 V to +0.6 V (vs Ag/AgCl) under AM1.5G (e) Nyquist plot measured at 0 V under AM1.5G

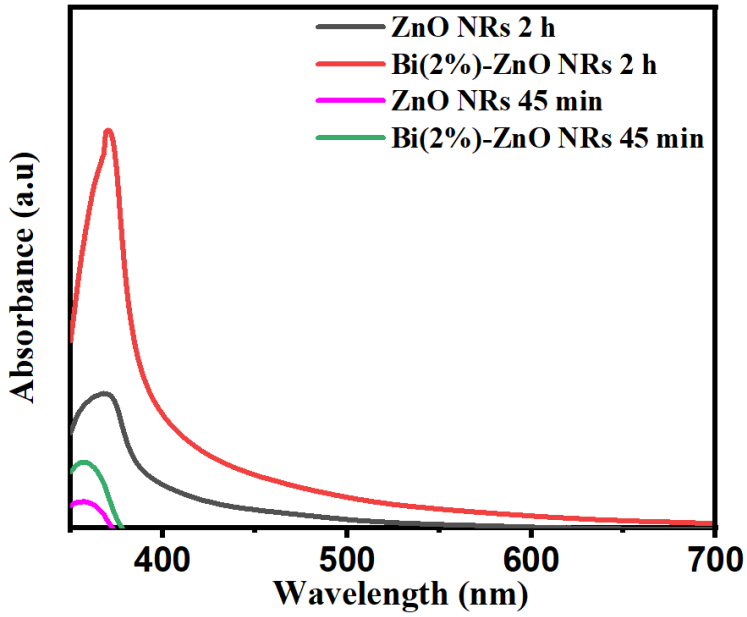

Figure 4.4: UV-vis spectra of ZnO NRs and Bi(2%)-ZnO NRs grown at 45 min and 2 h

4.2.2 PEC performance analysis

The effect of growth time on PEC performance was studied. ZnO NRs and Bi(2%)-ZnO NRs were both grown at 45 min and 2 h, and their respective PEC performance recorded as illustrated in Figure 4.5 (a)-(f). During analysis, the following key observations were made. Under visible light, Bi(2%)-ZnO NRs (2 h) do have highest photocurrent based on possible afore-stated rationale. Under UV, ZnO NRs (2 h) performed barely better than ZnO NRs(45 min) which could be linked to multiphoton absorption due to light scattering as supported by UV-vis spectra data. Under AM1.5G, it seems there is a tie in photocurrent between ZnO NRs(45 min) and Bi(2%)-ZnO NRs(2 h). This could be a result of the trade-off between increased light absorption and increased recombination due to increased length by increasing growth time. This finding is supported by the LSV data measured under AM1.5G**,** the curves delineating ZnO NRs(45 min) and Bi(2%)-ZnO NRs (2 h) overlaps at +0.4 V—the applied voltage used to generate their respective photocurrents—thereby supporting the tie in photocurrent of both materials as shown by CA AM1.5G result. To resolve the dilemma in the photocurrent values between Bi(2%) 2 h and Bi(0%) 45 min, the Nyquist curves in Figure 4.5 (f) were fitted on an equivalent circuit as shown in Figure 4.6 (c). This approach was used because CA measurement is biased to applied voltage. However, Impedance curve and modeling provide the amazing opportunity of modeling the physical parts and processes thereby giving a good picture of underlying phenomena of the material. The parameters of the models are R_s, R_p, R_{ct}, C_{dl}, C_c and W which are resistance of electrolyte solution, resistance of

polarization, resistance of charge transport via photoanode/electrolyte interface, capacitance of coatings, wurburg impedance. Wurburg impedance was integrated into the model to account for the depression of semicircles in Nyquist plot. The fitted parameters can be found in Figure A.3. Analysis of the fitted data showed two key insights. One, the polarization resistance $\mathbf{R_p}$ which models the corrosion of the various photoanodes is between 7 and 24 ohms—indicating that distribution of $\mathbf{R_p}$ for the materials has small variance which may be a result of the same electrolyte(0.5M Na_2SO_4) used for EIS measurement. Also, the relatively small value implies that the corrosion of the materials is high. Lastly, the charge carrier resistance is lowest for Bi(0%) 45 min and highest for Bi(2%) 45 min. This finding hereby suggests that Bi(0%) 45 min would have a higher photoresponse than Bi(2%) 2 h owing to lower recombination rate occasioned by lower characteristic length and more efficient charge transfer. This can be corroborated using LSV data as it was observed that photocurrent of ZnO NRs (45 min) reached saturation at a smaller voltage compared to Bi(2%)-ZnO NRs (2 h) suggesting better charge separation as detailed by the EIS data. Photostability test was carried out on these materials for 1 h. It can be affirmed that bismuth does not impart stability onto ZnO NRs. Materials grown at '2 h' are more stable than those of '45 min'. Holding the time constant, bismuth doped materials seem to degrade faster than their pristine counterpart.

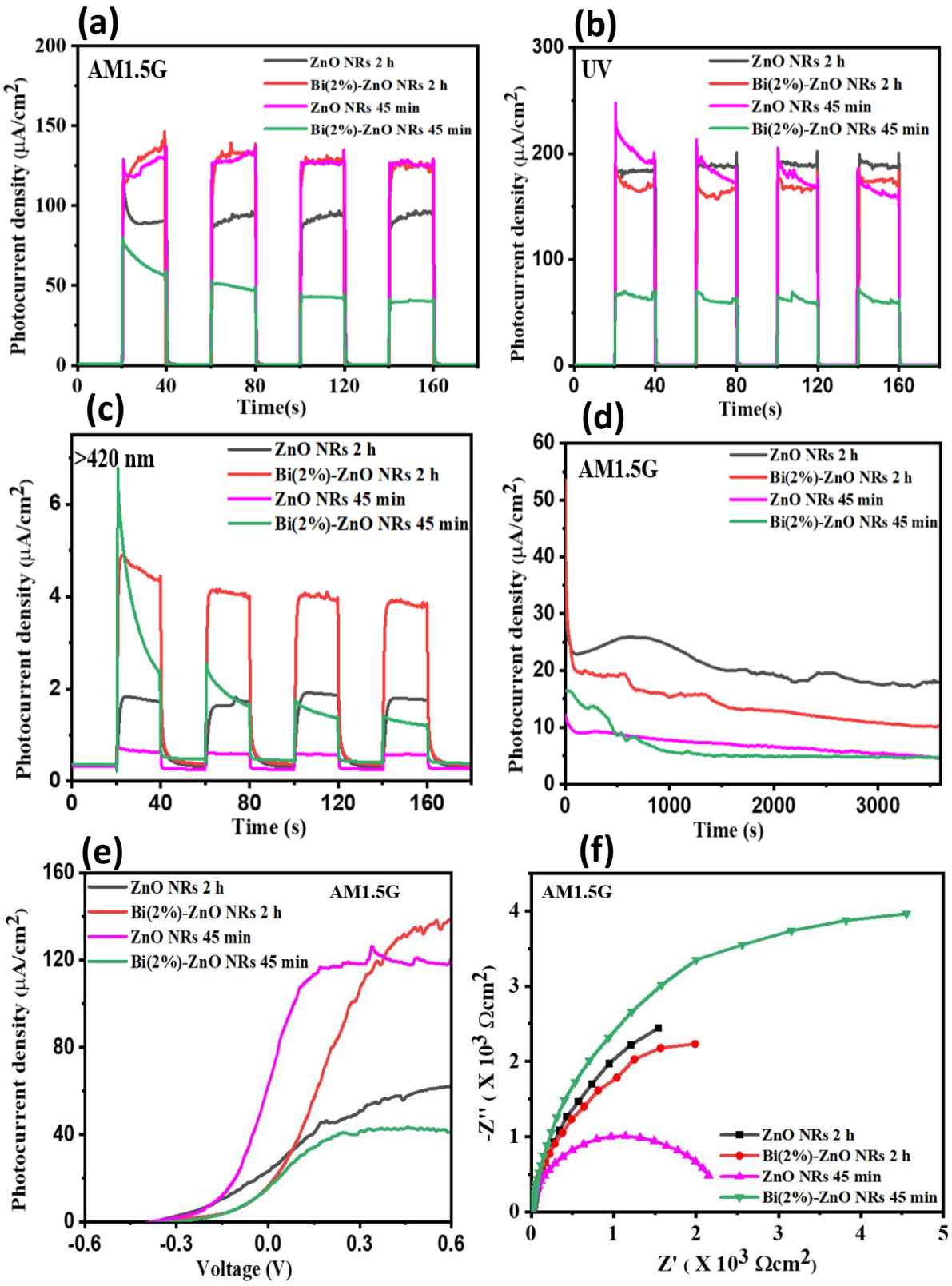

Figure 4.5: Plots for ZnO NRs and Bi(2%)-ZnO NRs with growth time 45 min and 2 h (a) CA AM1.5G (b) CA UV light (c) CA Visible(>420nm) light (d) CA photostability test performed for 1h under AM1.5G (e) LSV curves obtained with scan rate of 0.1 V/s and applied voltage

ranging from -0.6 V to +0.6 V (vs Ag/AgCl) under AM1.5G (f) Nyquist plot obtained at 0 V under AM1.5G

4.3 Comparison of 0.025M CB and Na_2SO_4 solution and impact on photoresponse and photostability of ZnO NRs

4.3.1 Photocurrent measurement

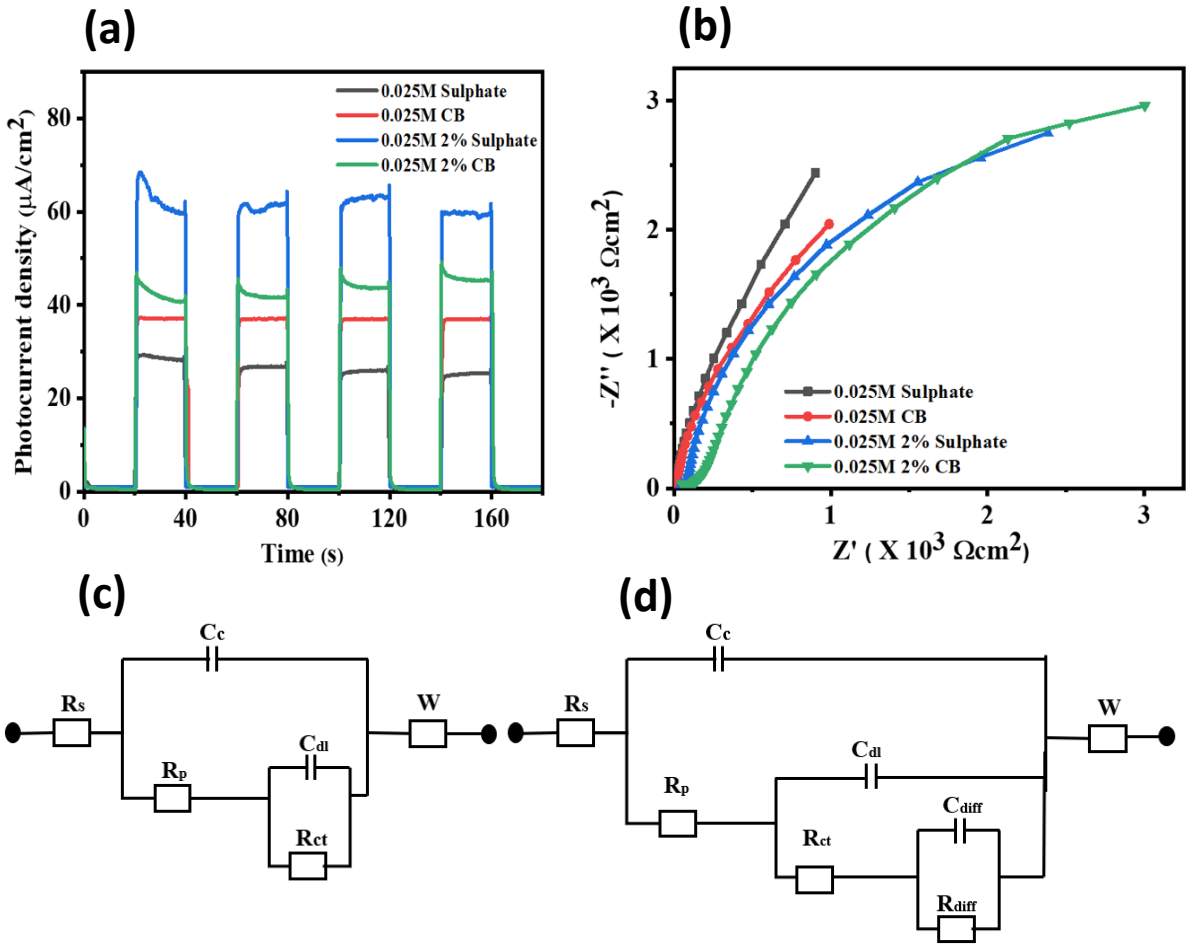

Figure 4.6: (a)-(b) CA and Nyquist plots of Bi(0, 2%)-ZnO NR in sulphate and CB under AM1.5G; Equivalent circuits for investigating electrochemical phenomena (c) with 2 RCs (d) with 3 RCs.

Figure 4.6 (a) shows various photocurrent responses to the doped and undoped materials for the first 3 min upon irradiation. It is interesting to observe a significant gain in photocurrent of materials for both electrolytes upon addition of bismuth. For sulphate and CB, 140% and 17% increase in photocurrent. To support this observation, EIS modeling was utilized to fit Nyquist curves for the respective materials in Figure 4.6 (b). The parameters of the models are R_s, R_p, R_{ct}, C_{dl}, C_c and W, R_{diff} and C_{diff} which are resistance of electrolyte solution, resistance

of polarization, resistance of charge transport via photoanode/electrolyte interface, capacitance of coatings, wurburg impedance, resistance and capacitance of diffusion respectively.

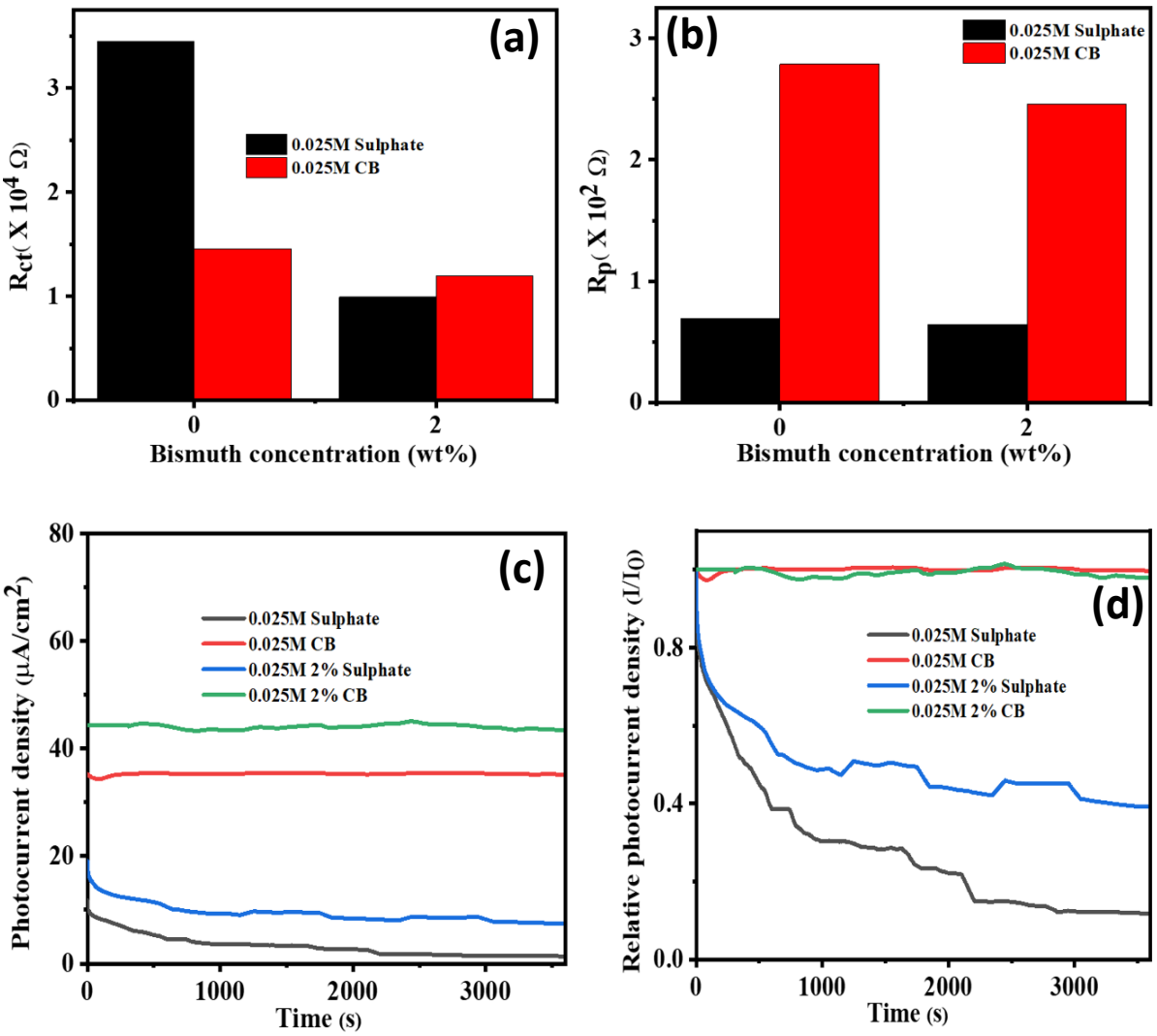

Figure 4.7: (a)-(b) Plots of charge carrier resistance vs bismuth concentration respectively; Photostability results (c) Photocurrent vs time (1 h) (d) Relative photocurrent density vs time (1 h)

It is important to note that the number of arcs in the Nyquist plot determines the number of RCs (resistance and capacitance circuits) to fit to the model[184]. 2RCs in Figure 4.6 (c) was used to fit 0.025M Sulphate, 0.025M 2% Sulphate and 0.025M CB while 3RCs in Figure 4.6 (d) was used to fit 0.025M 2% CB. This is because the former materials have impedance curves with 2 arcs while the latter has 3 arcs. The configuration of the RC model to be chosen was in accordance with the model in Njoku et al. report[185]. Figure A.4 shows the fitted parameters on Bi(0, 2%)-ZnO NRs in sulphate and CB solution. Based on the fitting of this curves, Figure

4.7 (a) revealed that R_{ct} seems to decrease with increase in bismuth concentration regardless of the electrolyte thereby suggesting better charge transport necessitated by increase in light absorption due to doping.

4.3.2 Photostability measurement

Figure 4.7 (c) and (d) compares the stability of the photoanodes. Bi(0, 2%)-ZnO NRs in CB have about 99% retainment in photocurrent after 1 h while those in sulphate electrolyte have 11% and 39% retainment in photocurrent after 1 h. This suggests that ZnO NRs in sulphate is less stable than in CB. EIS model showed that polarization resistance of CB is 4 times higher than that of sulphate indicating that there is more corrosive effect in sulphate.

Corrosion leads to dissolution of the materials which depends on the type of anions [186] and the pH of the solution[176]. The lowest solubility for ZnO has been reported to have a pH window between 9.9 and 12.3[187]. Accordingly, sulphate solution is expected to have higher solubility than CB because sulphate solution is a neutral solution with pH 7 while pH of CB is 10.5. It has also been garnered that SO_4^{2-} has a very high affinity for active Zn^{2+} polar sites leading to formation of passive layer which interferes with photocurrent generation and stability[188].

To further bolster this claim, a few studies have shown that buffered materials show superior performance compared to SO_4^{2-}-based materials. This fascinating property is because of the ability to donate/accept proton and hydroxyl ion in order to stabilize the concentration gradient of the bulk solution. This concentration gradient could have been changed by oxygen formation reaction leading to preservation of surface pH and thereby promoting water splitting[189].

Essentially, For CB, CO_3^{2-} protects the surface of the photoanode by serving as the “holes mediator” which prevents the availability of hydroxyl ion for the precipitation of sodium zincate while using it for balancing of the surface pH for efficient PEC activity[176].

To evaluate these chemical processes, SEM images of the photoanodes were observed as shown in Figure 4.8. By keen observation, there is no obvious damage done to the material under sulphate solution and CB. Albeit expected for CB due to its protective effort that minimizes the amount of zincate precipitate formed. Nevertheless, meticulous observation showed a relatively large size for photoanodes in sulphate solution due to adsorption of SO_4^{2-} on surface site — this is evidenced by numerical data of size distribution as shown in Figure A.5. It is noteworthy to mention that the lack of obvious damage could be attributed to low

concentration employed in this study leading to the delivery of a small amount of SO_4^{2-} species to the material surface.

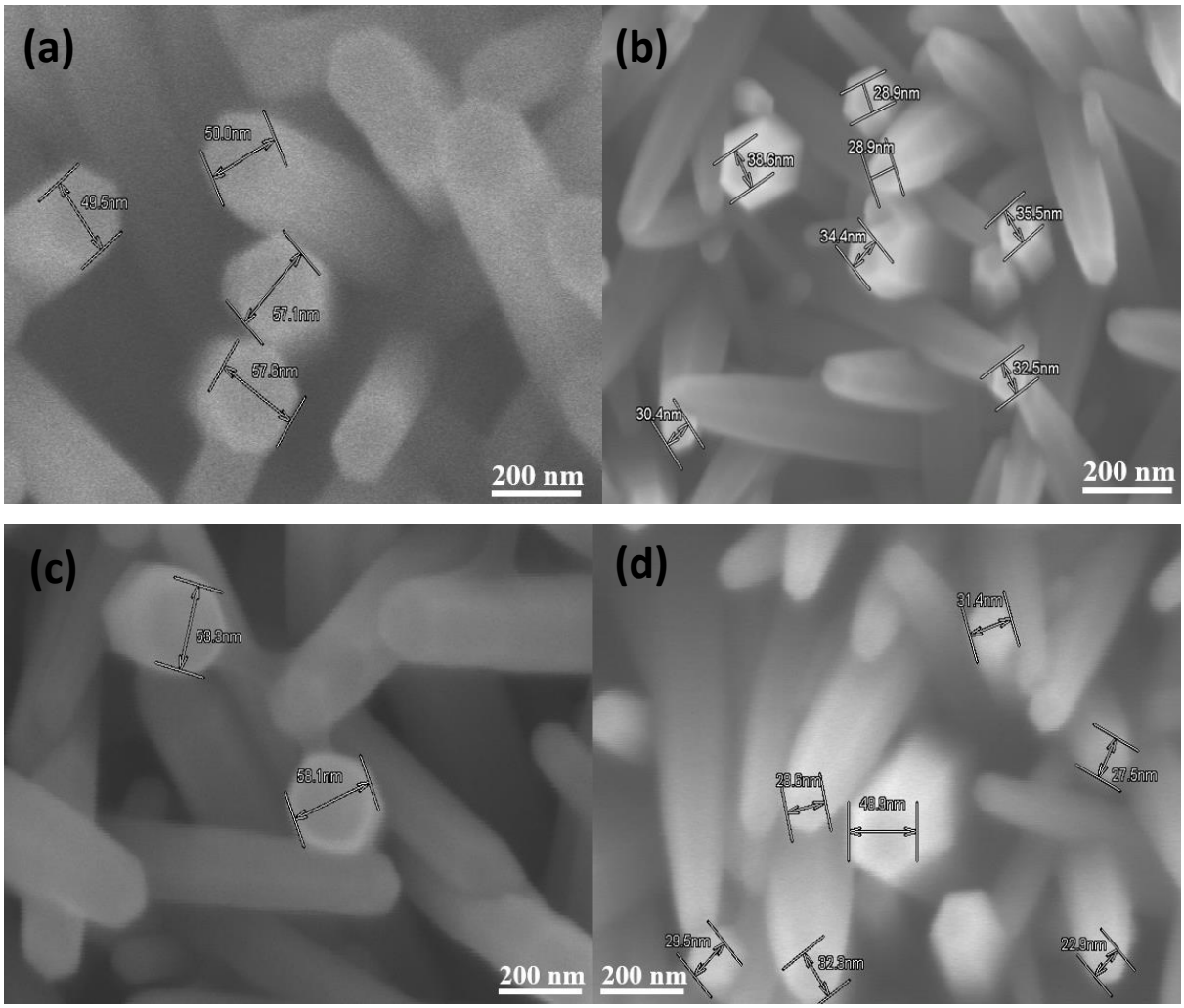

Figure 4.8: SEM Images (a)-(b) ZnO NR after 1 h of photostability test in 0.025M Sulphate and CB solution (c)-(d) Bi(2%)-ZnO NR photostability test in 0.025M Sulphate and CB solution

Chapter 5 Conclusion

Following the battery of experimental works, data collection and analysis performed for this project, a few assertions can be made:

1) For 2 h growth time, Bi(2%)-ZnO NRs has the highest photocurrent in visible and AM1.5G because of a host of factors such as highest vertical alignment of rods, highest light absorption, relatively low defects, reduced bandgap and least charge carrier resistance in the photoanode/electrolyte interface.
2) ZnO NRs (45 min) has the highest charge carrier efficiency when compared to Bi(2%)-ZnO NRs (2 h) because the latter has a higher recombination rate due to defects(bismuth-induced defects and native defects) and increase in characteristic length.
3) For “2 h” materials, the gain in photocurrent of ZnO NRs resulting from addition of 2%wt bismuth can be lost to photostability issues as determined by corrosive nature of 0.5M sulphate solution.
4) The loss in photocurrent by Bi(2%)-ZnO NRs (2 h) can be effectively preserved over a 1 h period by using stable electrolyte such as 0.025M carbonated buffer.

Chapter 6 Recommendation for Future work

This study has added to the body of knowledge affirming the incredible usefulness of doping as a strategic approach towards enhancing water-splitting effect of ZnO nanorods. At the same time, it has also showed that 0.025M carbonated buffer is effective at preserving photocurrents of not only pristine ZnO but also doped ZnO nanomaterials.

The usefulness of this work is not immediately obvious for commercial applications considering the relatively low level of photocurrents generated by the material. However, from experimental standpoint, it might be necessary to try to push investigation further by doing the following

1) Use advanced characterization techniques to investigate the interaction of dopants with ZnO lattice This could be achieved by evaluating phase change, composition, and nature of phases. This is necessary to propose mechanics for the self-assembly of crystal structures upon bismuth addition and possibly if there is a change in nature of self-assembly based on doping levels.
2) To shed more light on photostability of ZnO nanorods in the electrolytes used in the study. It would be necessary to gain more insight by using Inductively Coupled Plasma Time-of-Flight Mass Spectrometer (ICP-ToF-MS) to know the amount of Zn species in the electrolyte (this is necessary to determine the corrosive level of the electrolytes); Time-of-Flight Secondary Ion Mass Spectrometry (ToF-SIMS) for determining the protective nature of electrolytes by examining the intensity of characteristic ions of the electrolytes on the surface of the material.

Appendix

A.1

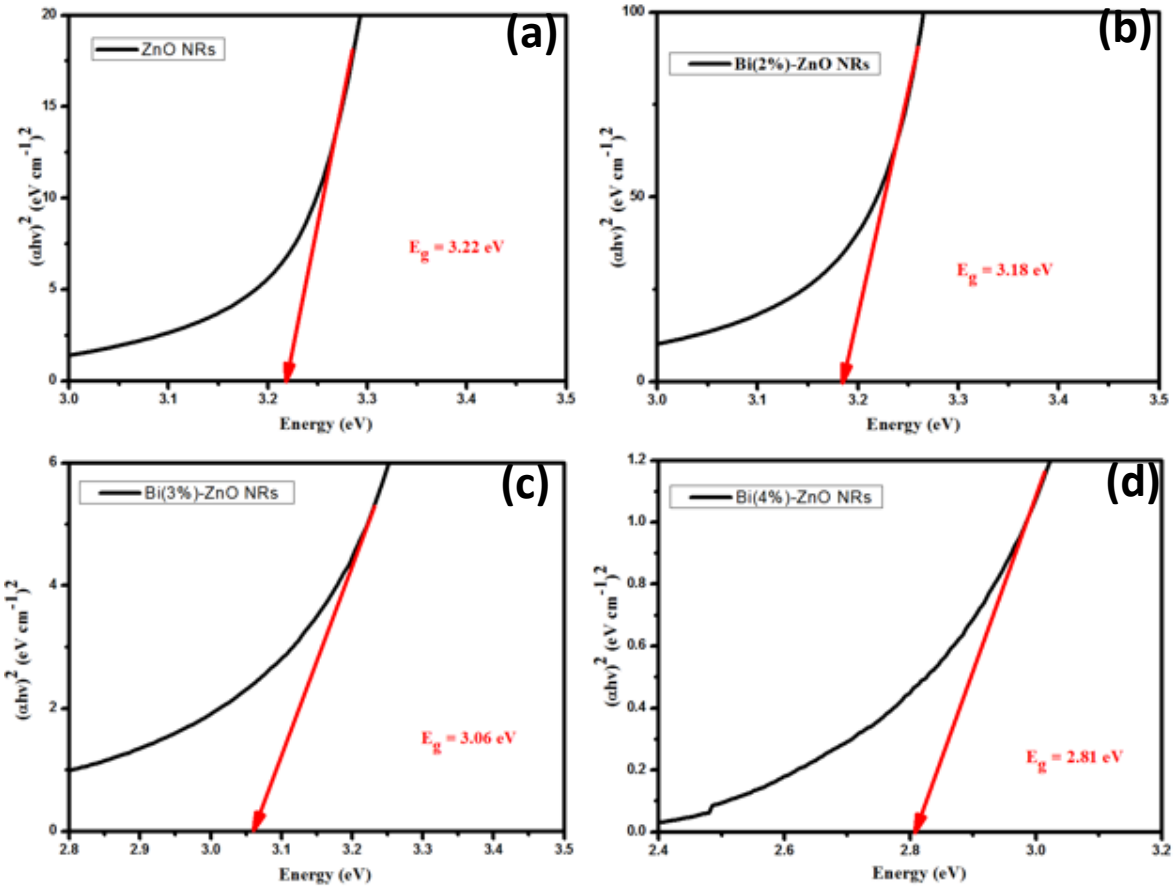

Figure A.1: Tauc plots detailing bandgap of Bi(0-4%)-ZnO NRs

A.2

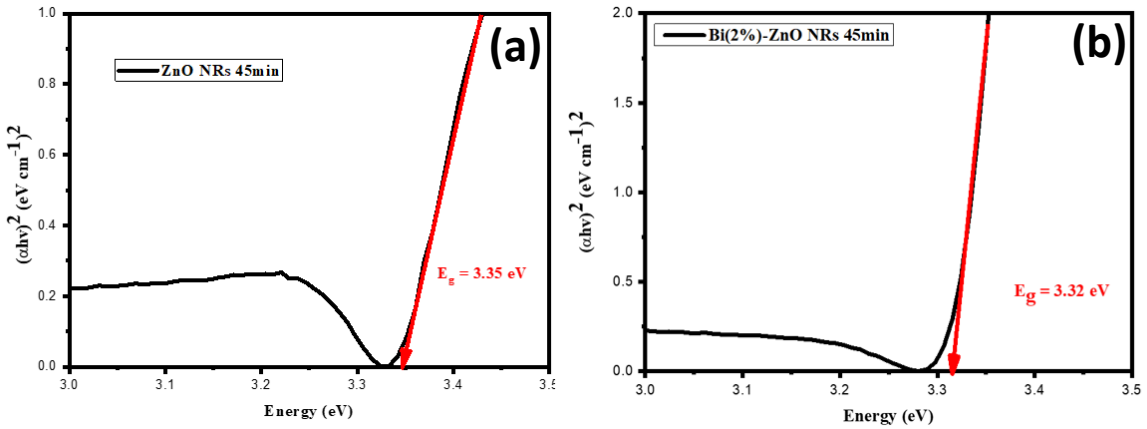

Figure A.2: (a)-(b) Tauc plot of ZnO NRs and Bi(2%)-ZnO NRs grown at 45 min

A.3

Sample	R_s (Ω)	R_p (Ω)	R_{ct} (Ω)	C_c (µF)	C_{dl} (µF)	W (× 10^{-6})
ZnO NR 2h	5.292	24.49	8080	1.13	27.83	1133
Bi(2%)-ZnO NR 2h	4.913	9.402	7056	0.1	18.81	3315
ZnO NR 45min	5.063	14.53	3778	1.02	6.86	1715
Bi(2%)-ZnO NR 45min	6.137	7.29	18580	1.05	5.22	497.7

Figure A.3: Fitted parameters of the equivalent circuits fitted to Bi(0, 2%)-ZnO NRs grown for 45 min and 2 h

A.4

Sample	R_s (Ω)	R_p (Ω)	R_{ct} (KΩ)	C_c (µF)	C_{dl} (µF)	R_{diff}(Ω)	C_{diff} (µF)	W (× 10^{-6})
0.025M Sulphate	46.39	69.07	34.5	0.3202	29.72			899.7
0.025M CB	113.3	278.9	14.54	0.25	25.09			433.9
2% 0.025 Sulphate	48.57	64.3	9.922	1.878	25.59			1114
2% 0.025M CB	50.27	245.7	11.93	0.028	16.27	58.23	28.8	83.73

Figure A.4: Table on fitted parameters for Bi(0, 2%)-ZnO NRs in sulphate and CB solution

A.5

Samples	Size distribution (nm)	Average size (nm)
ZnO NR in Sulphate	45.9 – 61.3	52.8
ZnO NR in CB	28.1 – 43.5	35
Bi(2%)-ZnO NR in Sulphate	39 – 58.1	46
Bi(2%)-ZnO NR in CB	19.7 – 45	29.67

Figure A.5: Table showing size distribution of materials after 1 h photostability test

References

[1] Lam S, Sin J, Abdullah A Z and Mohamed A R 2014 Transition metal oxide loaded ZnO nanorods: Preparation, characterization and their UV-vis photocatalytic activities *Sep. Purif. Technol.*

[2] Roy P, Berger S and Schmuki P 2011 TiO_2 Nanotubes : Synthesis and Applications Angewandte 2904–39

[3] Lu X, Wang G, Zhai T, Yu M, Gan J, Tong Y and Li Y 2012 Hydrogenated TiO_2 Nanotube Arrays for Supercapacitors

[4] Chai S, Zhao G, Li P, Lei Y, Zhang Y and Li D 2011 Novel Sieve-Like SnO 2 / TiO_2 Nanotubes with Integrated Photoelectrocatalysis : Fabrication and Application for Efficient Toxicity Elimination of Nitrophenol Wastewater 18261–9

[5] Tio D, Tsuchiya H, Ghicov A, Schmuki P and Maca J M 2005 Dye-sensitized anodic TiO_2 nanotubes ´ **7** 1133–7

[6] Shinde P S, Betty C A, Bhosale P N, Lee W J and Patil P S 2011 Applied Surface Science Nanocoral architecture of TiO_2 by hydrothermal process : Synthesis and characterization *Appl. Surf. Sci.* **257** 9737–46

[7] Huang J, Cao Y, Liu Z, Deng Z, Tang F and Wang W 2012 Efficient removal of heavy metal ions from water system by titanate nanoflowers *Chem. Eng. J.* **180** 75–80

[8] Jiang Y, Li M, Ding R, Song D, Trevor M and Chen Z 2013 Enhanced the performance of dye-sensitized solar cells with a novel photoanode using TiO_2 nano flower clusters and nanoparticles $ *Mater. Lett.* **107** 210–3

[9] Kusior A, Wnuk A, Trenczek-Zajac A, Zakrzewska K and Radecka M 2015 TiO_2 nanostructures for photoelectrochemical cells (PECs) *Int. J. Hydrogen Energy* **40** 4936–44

[10] Yu K and Chen J 2009 Enhancing solar cell efficiencies through 1-D nanostructures *Nanoscale Res. Lett.* **4** 1–10

[11] Velmurugan R and Swaminathan M 2011 Solar Energy Materials & Solar Cells An efficient nanostructured ZnO for dye sensitized degradation of Reactive Red 120 dye under solar light *Sol. Energy Mater. Sol. Cells* **95** 942–50

[12] Zhang Y, Ram M K, Stefanakos E K and Goswami D Y 2013 Surface & Coatings Technology Enhanced photocatalytic activity of iron doped zinc oxide nanowires for water decontamination *Surf. Coat. Technol.* **217** 119–23

[13] Guo Y, Wang H, He C, Qiu L and Cao X 2009 Uniform Carbon-Coated ZnO Nanorods : Microwave-Assisted Preparation , Cytotoxicity , and Photocatalytic Activity **25** 4678–84

[14] Subash B, Krishnakumar B, Pandiyan V, Swaminathan M and Shanthi M 2012 An efficient nanostructured Ag_2S – ZnO for degradation of Acid Black 1 dye under day light illumination *Sep. Purif. Technol.* **96** 204–13

[15] Saravanan R, Shankar H, Prakash T, Narayanan V and Stephen A 2011 ZnO / CdO composite nanorods for photocatalytic degradation of methylene blue under visible light *Mater. Chem. Phys.* **125** 277–80

[16] Sakthivel S, Geissen S, Bahnemann D W, Murugesan V and Vogelpohl A 2002 Enhancement of photocatalytic activity by semiconductor heterojunctions : Fe_2O_3, WO_3 and CdS deposited on ZnO **148** 283–93

[17] Abed S, Bougharraf H, Bouchouit K, Sofiani Z, Derkowska-Zielinska B, Aida M S and Sahraoui B 2015 Influence of Bi doping on the electrical and optical properties of ZnO thin films *Superlattices Microstruct.* **85** 370–8

[18] Gerischer H 1977 On the stability of semiconductor electrodes against photodecomposition *J. Electroanal. Chem.* **82** 133–43

[19] Xia B Y, Yang P, Sun Y, Wu Y, Mayers B, Gates B, Yin Y, Kim F and Yan H 2003 One-Dimensional Nanostructures : Synthesis , Characterization , and Applications ** 353–89

[20] Wang Z L 2009 Ten years' venturing in ZnO nanostructures: From discovery to scientific understanding and to technology applications *Chinese Sci. Bull.* **54** 4021–34

[21] Segets D, Gradl J, Taylor R K and Vassilev V 2009 Absorbance Spectra for the Determination of ZnO Nanoparticle Size Distribution, Solubility *ACS Nano* **3** 1703–10

[22] Lu F, Cai W and Zhang Y 2008 ZnO hierarchical micro/nanoarchitectures: Solvothermal synthesis and structurally enhanced photocatalytic performance *Adv. Funct. Mater.* **18** 1047–56

[23] Zhou J, Xu N and Wang Z L 2006 Dissolving behavior and stability of ZnO wires in biofluids: A study on biodegradability and biocompatibility of ZnO nanostructures *Adv. Mater.* **18** 2432–5

[24] Chu S, Wang G, Zhou W, Lin Y, Chernyak L, Zhao J, Kong J, Li L, Ren J and Liu J 2011 Electrically pumped waveguide lasing from ZnO nanowires *Nat. Nanotechnol.* **6** 506–10

[25] Na J H, Kitamura M, Arita M and Arakawa Y 2009 Hybrid p-n junction light-emitting diodes based on sputtered ZnO and organic semiconductors *Appl. Phys. Lett.* **95** 19–22

[26] Sudhagar P, Kumar R S, Jung J H, Cho W, Sathyamoorthy R, Won J and Kang Y S 2011 Facile synthesis of highly branched jacks-like ZnO nanorods and their applications in dye-sensitized solar cells *Mater. Res. Bull.* **46** 1473–9

[27] Wang Z L, Yang R, Zhou J, Qin Y, Xu C, Hu Y and Xu S 2010 Lateral nanowire/nanobelt based nanogenerators, piezotronics and piezo-phototronics *Mater. Sci. Eng. R Reports* **70** 320–9

[28] Xu J, Han J, Zhang Y, Sun Y and Xie B 2008 Studies on alcohol sensing mechanism of ZnO based gas sensors *Sensors Actuators, B Chem.* **132** 334–9

[29] Ahn S E, Soo J L, Kim H, Kim S, Kang B H, Kim K H and Kim G T 2004 Photoresponse of sol-gel-synthesized ZnO nanorods *Appl. Phys. Lett.* **84** 5022–4

[30] Liu Y, Yan X, Kang Z, Li Y, Shen Y, Sun Y, Wang L and Zhang Y 2016 Synergistic Effect of Surface Plasmonic particles and Surface Passivation layer on ZnO Nanorods Array for Improved Photoelectrochemical Water Splitting *Sci. Rep.* **6** 1–7

[31] Barber J 2009 Photosynthetic energy conversion: Natural and artificial *Chem. Soc. Rev.* **38** 185–96

[32] Jia J, Seitz L C, Benck J D, Huo Y, Chen Y, Ng J W D, Bilir T, Harris J S and Jaramillo T F 2016 Solar water splitting by photovoltaic-electrolysis with a solar-to-hydrogen efficiency over 30% *Nat. Commun.* **7** 1–6

[33] Bu Y and Ao J P 2017 A review on photoelectrochemical cathodic protection semiconductor thin films for metals *Green Energy Environ.* **2** 331–62

[34] Maeda K and Domen K 2010 Photocatalytic water splitting: Recent progress and future challenges *J. Phys. Chem. Lett.* **1** 2655–61

[35] Paraschivescu A, Popa K, Colisnic D, Timco G, Cecal A, Paraschivescu A, Popa K, Colisnic D, Timco G and Singenerean L 2003 Radiolytic splitting of water molecules in the presence of some supramolecular compounds *J. Serbian Chem. Soc.* **68** 593–8

[36] Akkerman I, Janssen M, Rocha J and Wij H 2002 File8F871Ac72E7E47B28C71634E33603625.Pdf **27** 1195–208

[37] Lédé J, Lapicque F and Villermaux J 1983 Production of hydrogen by direct thermal decomposition of water *Int. J. Hydrogen Energy* **8** 675–9

[38] Ozgur U, Alivov Y, Liu C, Teke A, Reshchikov M A, Dogan S, Avrutin V, Cho S J and Morkoc H 2005 A comprehensive review of ZnO materials and devices *J. Appl. Phys.* **98**

[39] Ashrafi A and Jagadish C 2007 Review of zincblende ZnO: Stability of metastable ZnO phases *J. Appl. Phys.* **102**

[40] Jaffe J E, Pandey R and Kunz A B 1991 Electronic structure of the rocksalt-structure semiconductors ZnO and CdO *Phys. Rev. B* **43** 14030–4

[41] Daudin B, Feuillet G, Hübner J, Samson Y, Widmann F, Philippe A, Bru-Chevallier C, Guillot G, Bustarret E, Bentoumi G and Deneuville A 1998 How to grow cubic GaN with low hexagonal phase content on (001) SiC by molecular beam epitaxy *J. Appl. Phys.* **84** 2295–300

[42] Bates, C. H., White, W. B., & Roy R 1962 New high-pressure polymorph of zinc oxide *Science (80-.).* **137** 993–993

[43] Jiang, J. Z., Olsen, J. S., Gerward, L., Frost, D., Rubie, D., & Peyronneau J 2000 Structural stability in nanocrystalline ZnO *EPL (Europhysics Lett.* **50** 48

[44] Liu H, Ding Y, Somayazulu M, Qian J, Shu J, Häusermann D and Mao H K 2005 Rietveld refinement study of the pressure dependence of the internal structural parameter u in the wurtzite phase of ZnO *Phys. Rev. B - Condens. Matter Mater. Phys.* **71**

[45] Jamieson J C 1970 The phase behavior of simple compounds *Phys. Earth Planet. Inter.* **3** 201–3

[46] Decremps F, Pellicer-Porres J, Datchi F, Itié J P, Polian A, Baudelet F and Jiang J Z 2003 Trapping of cubic ZnO nanocrystallites at ambient conditions *Appl. Phys. Lett.* **81** 4820–2

[47] Wang Y, Zhang Y, Chang W J, Lu G L, Jiang J Z, Li Y C, Liu J and Hu T D 2005 Mn effect on wurtzite-to-cubic phase transformation in ZnO *J. Phys. Chem. Solids* **66** 1775–8

[48] Ashrafi A B M A, Ueta A, Avramescu A, Kumano H, Suemune I, Ok Y-W and Seong T-Y 2000 Growth and characterization of hypothetical zinc-blende ZnO films on GaAs(001) substrates with ZnS buffer layers *Appl. Phys. Lett.* **76** 550–2

[49] Lee G H, Kawazoe T and Ohtsu M 2005 Room temperature near-field photoluminescence of zinc-blend and wurtzite ZnO structures *Appl. Surf. Sci.* **239** 394–7

[50] Kim S-K, Jeong S-Y and Cho C-R 2003 Structural reconstruction of hexagonal to cubic ZnO films on Pt/Ti/SiO2/Si substrate by annealing *Appl. Phys. Lett.* **82** 562–4

[51] Chichvarina O, Herng T S, Phuah K C, Xiao W, Bao N, Feng Y P and Ding J 2015 Stable zinc-blende ZnO thin films: formation and physical properties *J. Mater. Sci.* **50** 28–33

[52] D.C. Look, D.C. Reynolds, J.R. Sizelove, R.L. Jones, C.W. Litton G C and W C H 1997 ELECTRICAL PROPERTIES OF BULK ZnO *Solid State Commun.* **105** 399–401

[53] Maeda K, Sato M, Niikura I and Fukuda T 2005 Growth of 2 inch ZnO bulk single crystal by the hydrothermal method **49**

[54] Look D C, Reynolds D C, Litton C W, Jones R L and Eason D B 2002 Characterization of homoepitaxial p-type ZnO grown by molecular beam epitaxy **1830** 9–12

[55] Ohtomo A and Tsukazaki A 2005 Pulsed laser deposition of thin films and superlattices based on ZnO

[56] Florescu D I, Mourokh L G, Pollak F H, Look D C, Cantwell G and Li X 2002 High spatial resolution thermal conductivity of bulk ZnO (0001) *J. Appl. Phys.* **91** 890–2

[57] Özgür Ü, Gu X, Chevtchenko S, Spradlin J, Cho S-J, Morkoç H, Pollak F H, Everitt H O, Nemeth B and Nause J E 2006 Thermal conductivity of bulk ZnO after different thermal treatments *J. Electron. Mater.* **35** 550–5

[58] Ohshima E, Ogino H, Niikura I, Maeda K, Sato M, Ito M and Fukuda T 2004 Growth of the 2-in-size bulk ZnO single crystals by the hydrothermal method *J. Cryst. Growth* **260** 166–70

[59] Mang A and Reimann K 1995 Band gaps, crystal-field splitting, spin-orbit coupling, and exciton binding energies in ZnO under hydrostatic pressure *Solid State Commun.* **94** 251–4

[60] Madelung O 2012 *Semiconductors—basic data* (Springer Science & Business Media)

[61] Nickel N H and Terukov E 2006 *Zinc Oxide-A Material for Micro-and Optoelectronic Applications: Proceedings of the NATO Advanced Research Workshop on Zinc Oxide as a Material for Micro-and Optoelectronic Applications, held in St. Petersburg, Russia, from 23 to 25 June 2004* vol 194 (Springer Science & Business Media)

[62] Reynolds D C, Look D C and Jogai B 1996 Optically pumped ultraviolet lasing from ZnO *Solid State Commun.* **99** 873–5

[63] Bagnall D M, Chen Y F, Zhu Z, Yao T, Koyama S, Shen M Y and Goto T 1997 Optically pumped lasing of ZnO at room temperature *Appl. Phys. Lett.* **70** 2230–2

[64] Huang M H, Mao S, Feick H, Yan H, Wu Y, Kind H, Weber E, Russo R and Yang P 2001 Room-temperature ultraviolet nanowire nanolasers *Science (80-.).* **292** 1897–9

[65] Cao H, Zhao Y G, Ho S T, Seelig E W, Wang Q H and Chang R P H 1999 Random laser action in semiconductor powder *Phys. Rev. Lett.* **82** 2278

[66] Tsukazaki A, Ohtomo A, Onuma T, Ohtani M, Makino T, Sumiya M, Ohtani K, Chichibu S F, Fuke S, Segawa Y and others 2005 Repeated temperature modulation epitaxy for p-type doping and light-emitting diode based on ZnO *Nat. Mater.* **4** 42–6

[67] Ryu Y R, Kim W J and White H W 2000 Fabrication of homostructural ZnO p--n junctions *J. Cryst. Growth* **219** 419–22

[68] Chu S, Olmedo M, Yang Z, Kong J and Liu J 2008 Electrically pumped ultraviolet ZnO diode lasers on Si *Appl. Phys. Lett.* **93** 181106

[69] Ohshima E, Ogino H, Niikura I, Maeda K, Sato M, Ito M and Fukuda T 2004 Growth of the 2-in-size bulk ZnO single crystals by the hydrothermal method *J. Cryst. Growth* **260** 166–70

[70] Look D C, Reynolds D C, Sizelove J R, Jones R L, Litton C W, Cantwell G and Harsch W C 1998 Electrical properties of bulk ZnO *Solid State Commun.* **105** 399–401

[71] Reynolds D C, Litton C W, Look D C, Hoelscher J E, Claflin B, Collins T C, Nause J and Nemeth B 2004 High-quality, melt-grown ZnO single crystals *J. Appl. Phys.* **95** 4802–5

[72] Nause J and Nemeth B 2005 Pressurized melt growth of ZnO boules *Semicond. Sci. Technol.* **20** S45

[73] Ive T, Ben-Yaacov T, de Walle C G, Mishra U K, DenBaars S P and Speck J S 2008 Step-flow growth of ZnO (0 0 0 1) on GaN (0 0 0 1) by metalorganic chemical vapor epitaxy *J. Cryst. Growth* **310** 3407–12

[74] Ardakani H K 1996 Electrical conductivity of in situ “hydrogen-reduced” and structural properties of zinc oxide thin films deposited in different ambients by pulsed excimer laser ablation *Thin Solid Films* **287** 280–3

[75] Heinze S, Krtschil A, Bläsing J, Hempel T, Veit P, Dadgar A, Christen J and Krost A 2007 Homoepitaxial growth of ZnO by metalorganic vapor phase epitaxy in two-dimensional growth mode *J. Cryst. Growth* **308** 170–5

[76] H S S and Y W 1997 *Phosphor Handbook* (Phosphor Research Society (Boca Raton, FL: CRC Press))

[77] Cardona M and Peter Y Y 2005 *Fundamentals of semiconductors* (Springer)

[78] Eda K 1989 Zinc oxide varistors *IEEE Electr. Insul. Mag.* **5** 28–30

[79] Nanto H, Sokooshi H and Usuda T 1991 Smell sensor using zinc oxide thin films prepared by magnetron sputtering *TRANSDUCERS’91: 1991 International Conference on Solid-State Sensors and Actuators. Digest of Technical Papers* pp 596–9

[80] Schmidt O, Kiesel P, de Walle C G, Johnson N M, Nause J and Döhler G H 2005 Effects of an electrically conducting layer at the zinc oxide surface *Jpn. J. Appl. Phys.* **44** 7271

[81] Schmidt O, Geis A, Kiesel P, de Walle C G, Johnson N M, Bakin A, Waag A and Döhler G H 2006 Analysis of a conducting channel at the native zinc oxide surface *Superlattices Microstruct.* **39** 8–16

[82] Look D C 2007 Quantitative analysis of surface donors in ZnO *Surf. Sci.* **601** 5315–9

[83] Kamalasanan M N and Chandra S 1996 Sol-gel synthesis of ZnO thin films *Thin Solid Films* **288** 112–5

[84] Andrade E, Miki-Yoshida M and others 1999 Growth, structure and optical characterization of high quality ZnO thin films obtained by spray pyrolysis *Thin Solid Films* **350** 192–202

[85] Funakubo H, Mizutani N, Yonetsu M, Saiki A and Shinozaki K 1999 Orientation control of ZnO thin film prepared by CVD *J. Electroceramics* **4** 25–32

[86] Sakurai K, Kanehiro M, Nakahara K, Tanabe T, Fujita S and Fujita S 2000 Effects of oxygen plasma condition on MBE growth of ZnO *J. Cryst. Growth* **209** 522–5

[87] Zhang Y, Ram M K, Stefanakos E K and Goswami D Y 2012 Synthesis, Characterization, and Applications of ZnO Nanowires *J. Nanomater.* **2012** 1–22

[88] Gyu-Chul Yi C W and W I P 2005 ZnO nanorods: synthesis, characterization and applications *Semicond. Sci. Technol.* **20** S22–S34

[89] Kitamura K, Yatsui T, Ohtsu M and Yi G C 2008 Fabrication of vertically aligned ultrafine ZnO nanorods using metal-organic vapor phase epitaxy with a two-temperature growth method *Nanotechnology* **19** 17–20

[90] Tien L C, Pearton S J, Norton D P and Ren F 2008 Synthesis and microstructure of vertically aligned ZnO nanowires grown by high-pressure-assisted pulsed-laser deposition *J. Mater. Sci.* **43** 6925–32

[91] Petersen E W, Likovich E M, Russell K J and Narayanamurti V 2009 Growth of ZnO nanowires catalyzed by size-dependent melting of Au nanoparticles *Nanotechnology* **20**

[92] Ashraf S, Jones A C, Bacsa J, Steiner A, Chalker P R, Beahan P, Hindley S, Odedra R, Williams P A and Heys P N 2011 MOCVD of vertically aligned ZnO nanowires using bidentate ether adducts of dimethylzinc *Chem. Vap. Depos.* **17** 45–53

[93] Wang J S, Yang C S, Chen P I, Su C F, Chen W J, Chiu K C and Chou W C 2009 Catalyst-free highly vertically aligned ZnO nanoneedle arrays grown by plasma-assisted molecular beam epitaxy *Appl. Phys. A Mater. Sci. Process.* **97** 553–7

[94] Wang L, Zhang X, Zhao S, Zhou G, Zhou Y and Qi J 2005 Synthesis of well-aligned ZnO nanowires by simple physical vapor deposition on c -oriented ZnO thin films without catalysts or additives *Appl. Phys. Lett.* **86** 86–9

[95] Protasova L N, Rebrov E V., Choy K L, Pung S Y, Engels V, Cabaj M, Wheatley A E H and Schouten J C 2011 ZnO based nanowires grown by chemical vapour deposition for selective hydrogenation of acetylene alcohols *Catal. Sci. Technol.* **1** 768–77

[96] Liu B and Zeng H C 2003 Hydrothermal Synthesis of ZnO Nanorods in Diameter Regime of 50 nm (Supporting Information) *J. Am. Chem. Soc.* 2–3

[97] An G, Sun Z, Zhang Y, Ding K, Xie Y, Tao R, Zhang H and Liu Z 2011 CO 2 -

Mediated Synthesis of ZnO Nanorods and Their Application in Sensing Ethanol Vapor *J. Nanosci. Nanotechnol.* **11** 1252–8

[98] Sugunan A, Warad H C, Boman M and Dutta J 2006 Zinc oxide nanowires in chemical bath on seeded substrates: Role of hexamine *J. Sol-Gel Sci. Technol.* **39** 49–56

[99] Pokai S, Limnonthakul P, Horprathum M, Eiamchai P, Pattantsetakul V, Limwichean S, Nuntawong N, Porntheeraphat S and Chitichotpanya C 2017 Influence of seed layer thickness on well-aligned ZnO nanorods via hydrothermal method *Mater. Today Proc.* **4** 6336–41

[100] Ladanov M, Ram M K, Matthews G and Kumar A 2011 Structure and opto-electrochemical properties of ZnO nanowires grown on n-Si substrate *Langmuir* **27** 9012–7

[101] Govender K, Boyle D S, Kenway P B and O'Brien P 2004 Understanding the factors that govern the deposition and morphology of thin films of ZnO from aqueous solutionElectronic supplementary information (ESI) available: Fig. A,B: film thickness profiles for Zn?en and Zn?TEA systems; Fig. C: SEM images of ZnO f *J. Mater. Chem.* **14** 2575–91

[102] Govender K, Boyle D S, Kenway P B and O'Brien P 2004 Understanding the factors that govern the deposition and morphology of thin films of ZnO from aqueous solution *J. Mater. Chem.* **14** 2575–91

[103] Rachamim, A. R., Dalal, S. H., Pfaendler, S. M.-L., Swanwick, M. E., Flewitt, A., & Milne W I 2009 Quantitative Investigation of the Factors Affecting the Hydrothermal Growth of Zinc Oxide Nanowires *MRS Proc.* **11** 1174

[104] Alshehri N A, Lewis A R, Pleydell-Pearce C and Maffeis T G G 2018 Investigation of the growth parameters of hydrothermal ZnO nanowires for scale up applications *J. Saudi Chem. Soc.* **22** 538–45

[105] Xu, S., Lao, C., Weintraub, B., & Wang Z L 2008 Density-controlled growth of aligned ZnO nanowire arrays by seedless chemical approach on smooth surfaces *J. Mater. Res.* **23** 2072–2077

[106] Kim A R, Lee J-Y, Jang B R, Lee J Y, Kim H S and Jang N W 2011 Effect of Zn²⁺ Source Concentration on Hydrothermally Grown ZnO Nanorods *J. Nanosci. Nanotechnol.* **11** 6395–9

[107] Yuan Z, Yu J and Jiang Y 2011 Growth of diameter-controlled zno nanorod arrays by hydrothermal technique for polymer solar cell application *Energy Procedia* **12** 502–7

[108] Baruah, S. & D 2009 Effect of seeded substrates on hydrothermally grown ZnO nanorods *J. Sol-Gel Sci. Technol.* **50** 456–464

[109] Navarro Yerga R M, Alvarez-Galván M C, Vaquero F, Arenales J and Fierro J L G 2013 Hydrogen Production from Water Splitting Using Photo-Semiconductor Catalysts *Renew. Hydrog. Technol. Prod. Purification, Storage, Appl. Saf.* 43–61

[110] Cho S, Jang J-W, Lee K-H and Lee J S 2014 Research Update: Strategies for efficient photoelectrochemical water splitting using metal oxide photoanodes *Apl Mater.* **2** 10703

[111] Yang Y, Xu D, Wu Q and Diao P 2016 Cu 2 O/CuO bilayered composite as a high-efficiency photocathode for photoelectrochemical hydrogen evolution reaction *Sci. Rep.* **6** 1–13

[112] Wu G, Tian M and Chen A 2012 Synthesis of CdS quantum-dot sensitized TiO2 nanowires with high photocatalytic activity for water splitting *J. Photochem. Photobiol. A Chem.* **233** 65–71

[113] Fujishima A H K 1972 Electrochemical photolysis of water at a semiconductor electrode *Nature* **238** 37–8

[114] Ahmad H, Kamarudin S K, Minggu L J and Kassim M 2015 Hydrogen from photo-catalytic water splitting process: A review *Renew. Sustain. Energy Rev.* **43** 599–610

[115] Wolcott A, Smith W A, Kuykendall T R, Zhao Y and Zhang J Z 2009 Photoelectrochemical study of nanostructured Zno thin films for hydrogen generation from water splitting *Adv. Funct. Mater.* **19** 1849–56

[116] Szymanski P and El-Sayed M A 2014 Some recent developments in photoelectrochemical water splitting using nanostructured TiO 2: a short review *Marco Antonio Chaer Nascimento* (Springer) pp 7–18

[117] Wilke T, Schricker D, Rolf J, Kleinermanns K and others 2012 Solar water splitting by semiconductor nanocomposites and hydrogen storage with quinoid systems *Open J. Phys. Chem.* **2** 195

[118] Li L, Liu C, Qiu Y, Mitsuzak N and Chen Z 2017 Convex-nanorods of $α$-Fe2O3/CQDs heterojunction photoanode synthesized by a facile hydrothermal method for highly efficient water oxidation *Int. J. Hydrogen Energy* **42** 19654–63

[119] Li J, Zhou J, Hao H and Li W 2017 Controlled synthesis of Fe2O3 modified Ag-010BiVO4 heterostructures with enhanced photoelectrochemical activity toward the dye degradation *Appl. Surf. Sci.* **399** 1–9

[120] Dong G, Du B, Liu L, Zhang W, Liang Y, Shi H and Wang W 2017 Synthesis and their enhanced photoelectrochemical performance of ZnO nanoparticle-loaded CuO dandelion heterostructures under solar light *Appl. Surf. Sci.* **399** 86–94

[121] Maeda K 2013 Z-scheme water splitting using two different semiconductor photocatalysts *Acs Catal.* **3** 1486–503

[122] Jo W-K and Sivakumar Natarajan T 2015 Facile synthesis of novel redox-mediator-free direct Z-scheme CaIn2S4 marigold-flower-like/TiO2 photocatalysts with superior photocatalytic efficiency *ACS Appl. Mater. Interfaces* **7** 17138–54

[123] Joy J, Mathew J and George S C 2018 Nanomaterials for photoelectrochemical water splitting – review *Int. J. Hydrogen Energy* **43** 4804–17

[124] Al-Agel F A, Suleiman J and Khan S A 2017 Studies on silicon quantum dots prepared at different working pressure *Results Phys.* **7** 1128–34

[125] Nie Q, Yang L, Cao C, Zeng Y, Wang G, Wang C and Lin S 2017 Interface optimization of ZnO nanorod/CdS quantum dots heterostructure by a facile two-step low-temperature thermal treatment for improved photoelectrochemical water splitting *Chem. Eng. J.* **325** 151–9

[126] Pokrant S, Dilger S, Landsmann S and Trottmann M 2017 Size effects of cocatalysts in photoelectrochemical and photocatalytic water splitting *Mater. Today Energy* **5** 158–63

[127] Gong J, Lai Y and Lin C 2010 Electrochemically multi-anodized TiO2 nanotube arrays for enhancing hydrogen generation by photoelectrocatalytic water splitting *Electrochim. Acta* **55** 4776–82

[128] de Krol R 2012 Principles of photoelectrochemical cells *Photoelectrochemical hydrogen production* (Springer) pp 13–67

[129] Wang C, Chen Z, Jin H, Cao C, Li J and Mi Z 2014 Enhancing visible-light photoelectrochemical water splitting through transition-metal doped TiO 2 nanorod arrays *J. Mater. Chem. A* **2** 17820–7

[130] Gupta N M 2017 Factors affecting the efficiency of a water splitting photocatalyst: a perspective *Renew. Sustain. Energy Rev.* **71** 585–601

[131] Yin W-J, Tang H, Wei S-H, Al-Jassim M M, Turner J and Yan Y 2010 Band structure engineering of semiconductors for enhanced photoelectrochemical water splitting: the case of TiO 2 *Phys. Rev. B* **82** 45106

[132] Yan H, Wang X, Yao M and Yao X 2013 Band structure design of semiconductors for enhanced photocatalytic activity: the case of TiO2 *Prog. Nat. Sci. Mater. Int.* **23** 402–7

[133] Wang J, Sun H, Huang J, Li Q and Yang J 2014 Band structure tuning of TiO2 for enhanced photoelectrochemical water splitting *J. Phys. Chem. C* **118** 7451–7

[134] Vishwakarma A K, Tripathi P, Srivastava A, Sinha A S K and Srivastava O N 2017 Band gap engineering of Gd and Co doped BiFeO3 and their application in hydrogen production through photoelectrochemical route *Int. J. Hydrogen Energy* **42** 22677–86

[135] Liu Z, Wu J and Zhang J 2016 Quantum dots and plasmonic Ag decorated WO3 nanorod photoanodes with enhanced photoelectrochemical performances *Int. J. Hydrogen Energy* **41** 20529–35

[136] Varadhan P, Fu H-C, Priante D, Retamal J R D, Zhao C, Ebaid M, Ng T K, Ajia I, Mitra S, Roqan I S and others 2017 Surface passivation of GaN nanowires for enhanced photoelectrochemical water-splitting *Nano Lett.* **17** 1520–8

[137] Momeni M M and Ghayeb Y 2015 Visible light-driven photoelectrochemical water splitting on ZnO--TiO 2 heterogeneous nanotube photoanodes *J. Appl. Electrochem.* **45** 557–66

[138] Fekete M, Riedel W, Patti A F and Spiccia L 2014 Photoelectrochemical water oxidation by screen printed ZnO nanoparticle films: effect of pH on catalytic activity and stability *Nanoscale* **6** 7585–93

[139] Walter M G, Warren E L, McKone J R, Boettcher S W, Mi Q, Santori E A and Lewis N S 2010 Solar Water Splitting Cells *Chem. Rev.* **110** 6446–73

[140] Yousefi M, Amiri M, Azimirad R and Moshfegh A Z 2011 Enhanced photoelectrochemical activity of Ce doped ZnO nanocomposite thin films under visible light *J. Electroanal. Chem.* **661** 106–12

[141] Chen L C, Lin Y G, Hsu Y K, Chen Y C, Chen S Y and Chen K H 2012 Visible-light-

driven photocatalytic carbon-doped porous ZnO nanoarchitectures for solar water-splitting *Nanoscale* **4** 6515–9

[142] Jaramillo T F, Baeck S-H, Kleiman-Shwarsctein A, Choi K-S, Stucky G D and McFarland E W 2005 Automated Electrochemical Synthesis and Photoelectrochemical Characterization of Zn1-x Co x O Thin Films for Solar Hydrogen Production *J. Comb. Chem.* **7** 264–71

[143] Sharma V, Kumar P, Shrivastava J, Solanki A, Satsangi V R, Dass S and Shrivastav R 2011 Vertically aligned nanocrystalline Cu--ZnO thin films for photoelectrochemical splitting of water *J. Mater. Sci.* **46** 3792–801

[144] Selloum D, Henni A, Karar A, Tabchouche A, Harfouche N, Bacha O, Tingry S and Rosei F 2019 Effects of Fe concentration on properties of ZnO nanostructures and their application to photocurrent generation *Solid State Sci.* **92** 76–80

[145] Wang F, Seo J H, Li Z, Kvit A V., Ma Z and Wang X 2014 Cl-doped ZnO nanowires with metallic conductivity and their application for high-performance photoelectrochemical electrodes *ACS Appl. Mater. Interfaces* **6** 1288–93

[146] Snigurenko D, Jakiela R, Guziewicz E, Przezdziecka E, Stachowicz M, Kopalko K, Barcz A, Lisowski W, Sobczak J W, Krawczyk M and Jablonski A 2014 XPS study of arsenic doped ZnO grown by Atomic Layer Deposition *J. Alloys Compd.* **582** 594–7

[147] Yuldashev S U, Panin G N, Kang T W, Nusretov R A and Khvan I V. 2006 Electrical and optical properties of ZnO thin films grown on Si substrates *J. Appl. Phys.* **100**

[148] Panigrahy B and Bahadur D 2012 P-type Phosphorus doped ZnO nanostructures: An electrical, optical, and magnetic properties study *RSC Adv.* **2** 6222–7

[149] Kang J W, Choi Y S, Choe M, Kim N Y, Lee T, Kim B J, Tu C W and Park S J 2012 Electrical and structural properties of antimony-doped p-type ZnO nanorods with self-corrugated surfaces *Nanotechnology* **23**

[150] Park C, Kim S and Lim S 2013 Synthesis of arsenic-doped p-type ZnO films by addition of As 2O3 to the ZnO spin coating solution *Solid State Commun.* **167** 18–22

[151] Lee J W, Subramaniam N G, Lee J C, Kumar S S and Kang T W 2011 Study of stable p-type conductivity in bismuth-doped ZnO films grown by pulsed-laser deposition *Epl* **95**

[152] Yang X, Wolcott A, Wang G, Sobo A, Fitzmorris R C, Qian F, Zhang J Z and Li Y 2009 Nitrogen-doped ZnO nanowire arrays for photoelectrochemical water splitting *Nano Lett.* **9** 2331–6

[153] Ahn K-S, Yan Y, Lee S-H, Deutsch T, Turner J, Tracy C E, Perkins C L and Al-Jassim M 2007 Photoelectrochemical Properties of N-Incorporated ZnO Films Deposited by Reactive RF Magnetron Sputtering *J. Electrochem. Soc.* **154** B956

[154] Yogeeswaran G, Chenthamarakshan C R, de Tacconi N R and Rajeshwar K 2006 Cadmium- and indium-doped zinc oxide by combustion synthesis using dopant chloride precursors *J. Mater. Res.* **21** 3234–41

[155] Shet S, Ahn K S, Deutsch T, Wang H, Nuggehalli R, Yan Y, Turner J and Al-Jassim M 2010 Influence of gas ambient on the synthesis of co-doped ZnO:(Al,N) films for photoelectrochemical water splitting *J. Power Sources* **195** 5801–5

[156] Shet S, Ahn K S, Nuggehalli R, Yan Y, Turner J and Al-Jassim M 2011 Phase separation in Ga and N co-incorporated ZnO films and its effects on photo-response in photoelectrochemical water splitting *Thin Solid Films* **519** 5983–7

[157] Duclère J R, O'Haire R, Meaney A, Johnston K, Reid I, Tobin G, Mosnier J P, Guilloux-Viry M, McGlynn E and Henry M O 2005 Fabrication of p-type doped ZnO thin films using pulsed laser deposition *J. Mater. Sci. Mater. Electron.* **16** 421–7

[158] Xiu F X, Mandalapu L J, Yang Z, Liu J L, Liu G F and Yarmoff J A 2006 Bi-induced acceptor states in ZnO by molecular-beam epitaxy *Appl. Phys. Lett.* **89** 2004–7

[159] Walter M G, Warren E L, McKone J R, Boettcher S W, Mi Q, Santori E A and Lewis N S 2010 Solar water splitting cells *Chem. Rev.* **110** 6446–73

[160] Zhang X G 2013 *Corrosion and electrochemistry of zinc* (Springer Science & Business Media)

[161] Bond A M 2002 *Broadening electrochemical horizons: principles and illustration of voltammetric and related techniques* (Oxford University Press on Demand)

[162] Chen S and Wang L-W 2012 Thermodynamic oxidation and reduction potentials of photocatalytic semiconductors in aqueous solution *Chem. Mater.* **24** 3659–66

[163] Pourbaix M Atlas of Electrochemical Equilibria in Aqueous Solutions

[164] Stumm W and Morgan J J 2012 *Aquatic chemistry: chemical equilibria and rates in natural waters* vol 126 (John Wiley & Sons)

[165] Klemm S O, Pust S E, Hassel A W, Hüpkes J and Mayrhofer K J J 2012 Electrochemical texturing of Al-doped ZnO thin films for photovoltaic applications *J. Solid State Electrochem.* **16** 283–90

[166] Pettinger B, Schöppel H-R, Yokoyama T and Gerischer H 1974 Tunnelling Processes at Highly Doped ZnO-Electrodes in Aqueous Electrolytes Part II: Electron Exchange with the Valence Band *Berichte der Bunsengesellschaft für Phys. Chemie* **78** 1024–30

[167] Justice D D and Hurd R M 1971 Electrochemical dissolution of ZnO single crystals *J. Electrochem. Soc.* **118** 1417

[168] Zhang X G 1996 Electrochemistry of zinc oxide *Corrosion and Electrochemistry of Zinc* (Springer) pp 93–124

[169] Fruhwirth O, Herzog G W, Hollerer I and Reitsamer G 1982 ZnO dissolution kinetics by means of A 65Zn tracer method *Surf. Technol.* **15** 43–50

[170] Gerischer H and Sorg N 1991 Chemical di'ssolution of oxides: Experiments with Sintered ZnO pellets and ZnO single crystals *Mater. Corros.* **42** 149–57

[171] Xiao F-X, Miao J, Tao H B, Hung S-F, Wang H-Y, Yang H Bin, Chen J, Chen R and Liu B 2015 One-dimensional hybrid nanostructures for heterogeneous photocatalysis and photoelectrocatalysis *Small* **11** 2115–31

[172] Wang R, Tan H, Zhao Z, Zhang G, Song L, Dong W and Sun Z 2014 Stable ZnO@ TiO 2 core/shell nanorod arrays with exposed high energy facets for self-cleaning coatings with anti-reflective properties *J. Mater. Chem. A* **2** 7313–8

[173] Lewis N S 1990 Mechanistic studies of light-induced charge separation at

semiconductor/liquid interfaces *Acc. Chem. Res.* **23** 176–83

[174] Kushwaha A and Aslam M 2014 Defect controlled water splitting characteristics of gold nanoparticle functionalized ZnO nanowire films *RSC Adv.* **4** 20955–63

[175] Xie S, Lu X and Tong Y 2013 An effective way to enhance photoelectrochemical photoactivity and stability of ZnO nanorod arrays by carbon and nitrogen co-treatment *Advanced Optoelectronics for Energy and Environment* pp ASa3A--28

[176] Liu C F, Lu Y J and Hu C C 2018 Effects of Anions and pH on the Stability of ZnO Nanorods for Photoelectrochemical Water Splitting *ACS Omega* **3** 3429–39

[177] Ginting R T, Lee H B, Tan S T, Tan C H, Jumali M H H, Yap C C, Kang J W and Yahaya M 2016 A Simple Approach Low-Temperature Solution Process for Preparation of Bismuth-Doped ZnO Nanorods and Its Application in Hybrid Solar Cells *J. Phys. Chem. C* **120** 771–80

[178] Chandrinou C, Boukos N, Stogios C and Travlos A 2009 PL study of oxygen defect formation in ZnO nanorods *Microelectronics J.* **40** 296–8

[179] Zeng H, Duan G, Li Y, Yang S, Xu X and Cai W 2010 Blue luminescence of ZnO nanoparticles based on non-equilibrium processes: Defect origins and emission controls *Adv. Funct. Mater.* **20** 561–72

[180] Peng W Q, Qu S C, Cong G W and Wang Z G 2006 Structure and visible luminescence of ZnO nanoparticles *Mater. Sci. Semicond. Process.* **9** 156–9

[181] Fan X M, Lian J S, Guo Z X and Lu H J 2005 Microstructure and photoluminescence properties of ZnO thin films grown by PLD on Si(1 1 1) substrates *Appl. Surf. Sci.* **239** 176–81

[182] Panigrahy B, Aslam M, Misra D S, Ghosh M and Bahadur D 2010 Defect-related emissions and magnetization properties of ZnO Nanorods *Adv. Funct. Mater.* **20** 1161–5

[183] Tan K H, Lim F S, Toh A Z Y, Zheng X X, Dee C F, Majlis B Y, Chai S P and Chang W S 2018 Tunable Spectrum Selectivity for Multiphoton Absorption with Enhanced Visible Light Trapping in ZnO Nanorods *Small* **14** 1–8

[184] Bredar A R C, Chown A L, Burton A R and Farnum B H 2020 Electrochemical Impedance Spectroscopy of Metal Oxide Electrodes for Energy Applications *ACS Appl. Energy Mater.* **3** 66–98

[185] Njoku D I, Cui M, Xiao H, Shang B and Li Y 2017 Understanding the anticorrosive protective mechanisms of modified epoxy coatings with improved barrier, active and self-healing functionalities: EIS and spectroscopic techniques *Sci. Rep.* **7** 1–15

[186] Gerischer H and Sorg N 1991 Chemical di'ssolution of oxides: Experiments with Sintered ZnO pellets and ZnO single crystals *Mater. Corros.* **42** 149–57

[187] Blok L and De Bruyn P L 1970 The ionic double layer at the ZnO solution interface. II. Composition model of the surface *J. Colloid Interface Sci.* **32** 527–32

[188] Fekete M, Riedel W, Patti A F and Spiccia L 2014 Photoelectrochemical water oxidation by screen printed ZnO nanoparticle films: Effect of pH on catalytic activity and stability *Nanoscale* **6** 7585–93

[189] Katsounaros I, Meier J C, Klemm S O, Topalov A A, Biedermann P U, Auinger M and Mayrhofer K J J 2011 The effective surface pH during reactions at the solid-liquid interface *Electrochem. commun.* **13** 634–7